


RESEARCH ARTICLE | APRIL 25 2023

Planar turbulent wakes under pressure gradient: Integral and self-similarity analyses

Tie Wei ; Xiaofeng Liu; Zhaorui Li; ... et. al



Physics of Fluids 35, 045149 (2023)

<https://doi.org/10.1063/5.0149652>

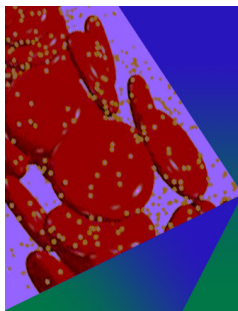


View
Online



Export
Citation

CrossMark



Physics of Fluids

Special Topic: Flow and Forensics

Submit Today!

Planar turbulent wakes under pressure gradient: Integral and self-similarity analyses

Cite as: Phys. Fluids **35**, 045149 (2023); doi: [10.1063/5.0149652](https://doi.org/10.1063/5.0149652)

Submitted: 7 March 2023 · Accepted: 6 April 2023 ·

Published Online: 25 April 2023






View Online



Export Citation



CrossMark

Tie Wei,^{1,a)}  Xiaofeng Liu,^{2,b)}  Zhaorui Li,^{3,c)}  and Daniel Livescu^{4,d)} 

AFFILIATIONS

¹Department of Mechanical Engineering, New Mexico Institute of Mining and Technology, 801 Leroy PL, Socorro, New Mexico 87801, USA

²Department of Aerospace Engineering, San Diego State University, San Diego, California 92182, USA

³Department of Engineering, Texas A&M University-Corpus Christi, 6300 Ocean Drive, Corpus Christi, Texas 78412, USA

⁴CCS-2, Los Alamos National Laboratory, Los Alamos, New Mexico 87545, USA

^{a)} Author to whom correspondence should be addressed: tie.wei@nmt.edu

^{b)} Electronic address: xiaofeng.Liu@sdsu.edu

^{c)} Electronic address: zhaorui.li@tamucc.edu

^{d)} Electronic address: livescu@lanl.gov

ABSTRACT

By using a combination of integral and self-similarity analyses, the generalized analytical solutions for the mean transverse velocity and Reynolds shear stress are rigorously derived for the first time for the far field of planar turbulent wakes under arbitrary pressure gradients. Specifically, by assuming self-similarity for the mean axial velocity, the analytical formulation for the mean transverse velocity is obtained from the integral of the mean continuity equation, and the analytical formulation for the Reynolds shear stress is obtained from the integral of the momentum equation. The generalized analytical formulations for the mean transverse velocity and Reynolds shear stress consist of multiple components, each with its unique scale and physical mechanism. In the zero pressure gradient limit, the generalized formulations recover the single-scale equations reported by Wei, Liu, and Livescu. Furthermore, simpler approximate formulations for the mean transverse velocity and Reynolds shear stress are also obtained, and show excellent agreement with the experimental measurements. The findings provide new insights into the properties of planar turbulent wakes under pressure gradients, filling some long-standing gaps in the existing literature.

Published under an exclusive license by AIP Publishing. <https://doi.org/10.1063/5.0149652>

I. INTRODUCTION

Turbulent wake flow is a commonly encountered type of free turbulent shear layer flow that has a wide range of applications in fields, such as aviation, sailing, combustion, propulsion, and environmental science. Despite extensive research on this subject, there is still a need to improve our understanding and ability to predict the behavior of turbulent wakes, especially under the influence of pressure gradients. In the present work, we use a combination of integral and self-similarity analyses to examine the impact of pressure gradients on planar turbulent wakes. Our findings identify new scales and lead to the development of new analytical equations that allow us to better understand the mean transverse flow and Reynolds shear stress and to clarify the effects of pressure gradients on these flows.

Turbulent wake flows with zero pressure gradient (ZPG) have been investigated for more than one hundred years. Comprehensive

reviews of the classic work on turbulent wake flows with zero pressure gradient can be found in the books of Schlichting,¹ Townsend,² and Pope.³ In practical applications, especially in aerodynamics, however, turbulent wakes are often subject to pressure gradients.⁴⁻⁷ In the multi-element airfoils used for high lift of transport aircraft, for instance, wake from an upstream element develops under a strong pressure gradient imposed by downstream elements. This is a critical issue in the aerodynamics design of multi-element airfoils, as flow reversals in the wake can result in significant reductions in the maximum lift, which is a key factor in determining the performance of transport aircraft.

Gartshore⁸ carried out an experimental study to understand the effect of pressure gradient on the development of wake flows. The sides of the wind tunnel were adjusted to bleed air to create an adverse pressure gradient (APG) when a perforated plate was fastened over the downstream of the section. In forming the wakes, the pressure

gradient downstream of a square rod was adjusted until an approximately constant ratio of $(U_e - U_{ctr})/U_e$ was obtained, where U_e is the free-stream velocity and U_{ctr} is the mean axial velocity at the wake centerline. Gartshore measured mean velocity, longitudinal and transverse turbulent intensity, intermittency and shear stress, and compared with Townsend's² data from small-deficit undistorted wakes.

To study the memory of the larger eddies in turbulent shear flow, Narasimha and Prabhu⁹ conducted experiments on planar turbulent wakes undergoing transition from an initial equilibrium state to a different final one, as a result of a nearly impulsive pressure gradient. They suggested that a flow satisfying the conditions required for a self-preservation analysis will exhibit equilibrium only if the relaxation length is small compared with a characteristic streamwise length scale of the flow.

Tummers *et al.*¹⁰ investigated the wake of a flat plate subjected to a strong adverse pressure gradient, which caused a local flow reversal and high turbulence intensities. The experimental data were used to determine terms in the turbulent kinetic energy equation. The comparison of experimental data with Reynolds-averaged Navier–Stokes simulation showed that both a $k - \epsilon$ model and a differential stress model predicted well the spreading rate of the wake, but predicted poorly the mean velocity and the turbulent kinetic energy on the wake centerline.

Liu and co-workers^{11–14} performed experimental investigations on the development of planar turbulent wakes subjected to adverse, zero, and favorable pressure gradient (FPG) conditions, respectively. The wake was generated by a flat splitter plate with tapered trailing edge, and the pressure gradients were imposed as the wake passed through a wind tunnel diffuser test section with fully adjustable top and bottom wall contours.^{11,12,14} The experiment's Reynolds number is 2.4×10^6 , based on the chord length of the wake generator. This value is similar to the Reynolds number for a wake flow that is produced by a leading-edge slat during the landing approach of a Boeing 737 aircraft. The streamwise pressure gradients imposed on the wake flow were held constant in each experiment: $dC_p/dx = 0.338 \pm 0.002/m$ under an adverse pressure gradient (APG), $dC_p/dx = 0.000 \pm 0.004/m$ under a constant-pressure or zero pressure gradient (ZPG), and $dC_p/dx = -0.60 \pm 0.01/m$ under a favorable pressure gradient (FPG). The pressure coefficient C_p is defined as $C_p = [P(x) - P_\infty]/q_\infty$, where $P(x)$ is the local static pressure in the diffuser, P_∞ and q_∞ are the static and dynamic pressures, respectively, upstream of the splitter plate. The mean velocity upstream of the wake generator was $U_{e0} = 30 \pm 0.2$ m/s. The use of constant pressure gradient, combined with identical initial conditions, facilitated isolation of the effect of streamwise pressure gradients on the evolution of the wake and provided a clean test bed for numerical simulations. The imposed pressure gradients were shown to have a significant effect on both the mean and turbulent flow statistics.

Driver and Mateer¹⁵ performed experiments of planar turbulent wake under an adverse pressure gradient in the High Reynolds Channel Number 1, a pressurized wind tunnel at NASA Ames Research Center. More details of the experiments are provided in a recent report.¹⁶ Driver and Mateer compared the experimental data with computational simulations using the turbulence models of Spalart and Allmaras¹⁷ and Menter.¹⁸ Computations with turbulence models fail to capture the flow reversals and the associated displacement effects observed in the experiment, but the performance of the simulation was improved by *ad hoc* increase in lag in the model.

Traditionally, the scale for the Reynolds shear stress (and Reynolds normal stresses) is assumed to be proportional to $(U_e - U_{ctr})^2$ (see, e.g., p. 198 in Ref. 2). However, such scaled Reynolds shear stress is found to vary with pressure gradient.¹² Based on a similarity analysis, Thomas and Liu¹⁴ found that incorporating the velocity defect with the streamwise rate of variation of product of the wake width and the local freestream velocity is better to capture the self-similarity of the Reynolds shear stress in planar turbulent wakes under pressure gradient. It is worth noting that in previous studies, the influence of pressure gradient on the mean transverse velocity has been largely omitted due to the scarcity of experimental data. Given its small magnitude, it is extremely challenging to obtain accurate experimental measurements of the mean transverse velocity. However, Liu *et al.*^{11,12} were able to measure the mean transverse velocity distribution with exceptional accuracy using hot wire. These experimental data are invaluable in validating the analytical derivations.

In the present work, we investigate the effects of pressure gradients on planar turbulent wake development using a combination of integral and self-similarity analyses. In Sec. II, the general characteristics of planar turbulent wakes under pressure gradient are described. Section III gives integral analyses of the mean continuity and momentum equations. New analytical equations are obtained to accurately predict the mean transverse velocity at the wake edge and the maximum Reynolds shear stress. In Sec. IV, new analytical equations are derived for the mean transverse velocity and Reynolds shear stress based on a self-similarity assumption of the mean axial velocity deficit. Simplified equations are also obtained to approximate the mean transverse velocity and Reynolds shear stress, showing excellent agreement with the experimental measurements of planar turbulent wakes under different pressure gradients. Section V summarizes the work.

II. GENERAL CHARACTERISTICS OF PLANAR TURBULENT WAKES SUBJECTED TO PRESSURE GRADIENT

The development of a planar turbulent wake is distinctively influenced by the pressure gradient. In the experiments of Liu,¹¹ the pressure gradient was created by adjusting the top and bottom walls of the diffuser test section, as depicted in Fig. 1 and detailed in Ref. 11. Sheet metal was used to construct the top and bottom walls, which can be modified using seven groups of turnbuckles. By adjusting the contour of the walls, Liu was able to optimize the conditions to create a constant pressure gradient as desired.

Figure 2 displays the mean axial velocity distribution in planar turbulent wakes under adverse pressure gradient, zero pressure gradient, and favorable pressure gradient. The data are from the experimental study of Liu.¹¹ Figure 2(a) presents the mean axial velocity in the dimensional form, and Fig. 2(b) presents the ratio of the mean axial velocity and the free stream velocity (adapted with permission from Fig. 3.8 of Ref. 11). The initial mean wake profiles are intentionally controlled in the experiments to be identical for different pressure gradients (see Fig. 3.2 in Ref. 11) and the free stream velocity is $U_{e0} = 30 \pm 0.2$ m/s. Figure 2(a) shows that, at a downstream location of $x = 30$ in., the free stream velocity U_e maintains at 30 m/s in the ZPG wake, but increases to about 35 m/s in the FPG wake and decreases to about 27.5 m/s in the APG wake. Figure 2(b) shows that the APG wake is wider and has a larger $U_e - U_{ctr}$ than that in the

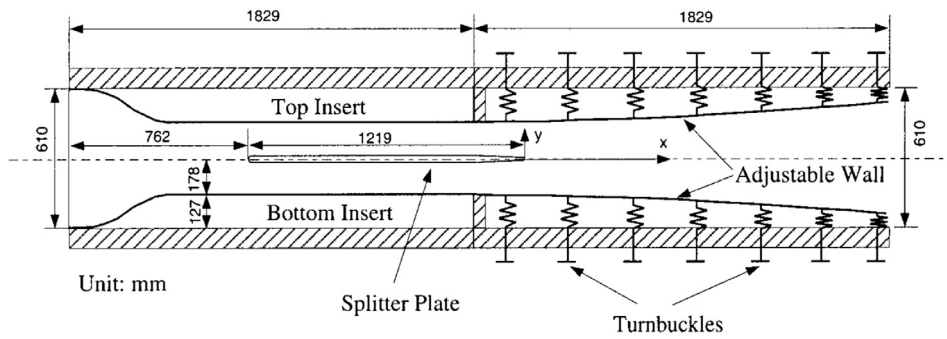


FIG. 1. Schematic of the test section in the experiments of Liu.¹¹ Reproduced with permission from X. Liu, "A study of wake development and structure in constant pressure gradients," Ph.D. thesis (University of Notre Dame, 2001) (Fig. 2.2).¹¹

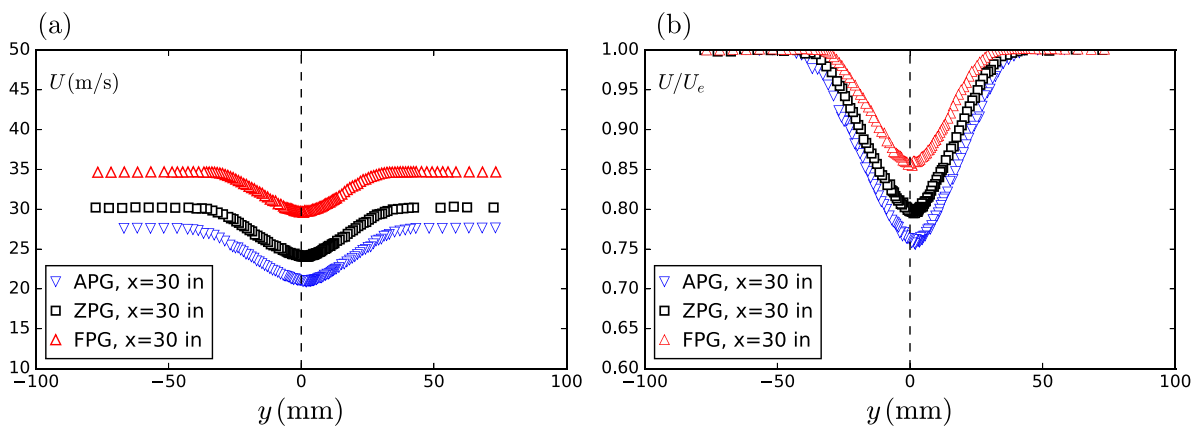


FIG. 2. Effects of pressure gradients on the mean axial velocity in planar wakes. Data are from experimental measurements of Liu¹¹ at $x = 30$ in. for APG wake, ZPG wake, and FPG wake. Reproduced with permission from X. Liu, "A study of wake development and structure in constant pressure gradients," Ph.D. thesis (University of Notre Dame, 2001) (Fig. 3.8).¹¹

ZPG wake. A favorable pressure gradient has the opposite effect on the variation of the wake width and the maximum axial velocity deficit.

The influence of pressure gradients on the wake spreading and velocity deficit decay rate has been documented in detail in Refs. 11–14. For the reader's convenience, the effects of pressure gradient on the wake width and mean axial velocity deficit are reproduced here. Following convention, the half-width of wake $\delta_{0.5}$ is defined as $U(y = \delta_{0.5}) = 0.5(U_e + U_{ctr})$. It is known (see Ref. 3, for example) that in a ZPG wake, the growth of the wake half-width in the far field can be approximated by a power law of $\delta_{0.5} \propto x^{0.5}$. Figure 3(a) shows that the wake half-width in the APG wake grows much faster than that in the ZPG or FPG wake.

For a planar turbulent ZPG wake, the decaying rate of the maximum mean axial velocity deficit can be approximate by a power law of $(U_e - U_{ctr})/U_e \propto x^{-0.5}$ (see Ref. 3, for example). Figure 3(b) shows that the ratio $(U_e - U_{ctr})/U_e$ decreases more rapidly in the FPG wake than in the ZPG wake. For the APG wake in Liu's experiment, the ratio remains roughly a constant of 0.25 in the range of 0.7–1.2 m and starts to increase slightly toward the end of the domain of investigation at $x = 1.4$ m.

III. INTEGRAL ANALYSIS OF PLANAR TURBULENT WAKES UNDER PRESSURE GRADIENT

In this section, integral analyses are carried out to determine the mean transverse velocity at the wake edge, and the maximum Reynolds shear stress in planar turbulent wake flow under pressure gradient. This work considers incompressible, single phase flows, and density is assumed to be constant. The governing equations for the mean flow in a planar turbulent wake are (see Eq. 6.2.9 in Ref. 2 or Eq. 5.55 in Ref. 3, for example) as follows:

$$0 = \frac{\partial U}{\partial x} + \frac{\partial V}{\partial y}, \quad (1a)$$

$$0 = -U \frac{\partial U}{\partial x} - V \frac{\partial U}{\partial y} - \frac{d(P/\rho)}{dx} + \frac{\partial R_{uv}}{\partial y} + \frac{\partial (R_{uu} - R_{vv})}{\partial x} + \nu \left\{ \frac{\partial^2 U}{\partial x^2} + \frac{\partial^2 U}{\partial y^2} \right\}. \quad (1b)$$

Here, x denotes the axial direction and y denotes the transverse direction. Upper case letters U and V denote the mean velocity in the axial and transverse directions, respectively. ρ is the fluid density and ν is

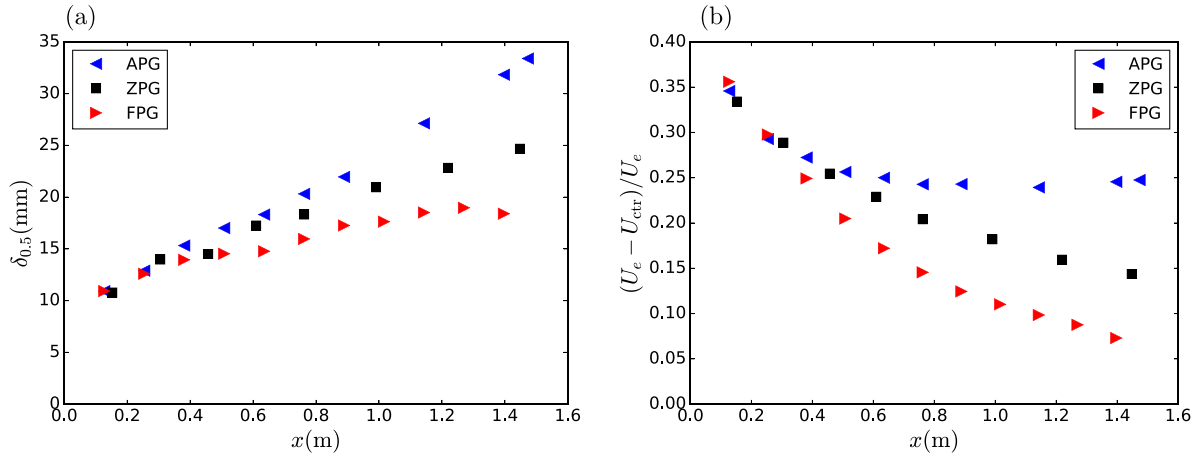


FIG. 3. (a) Growth of the wake half width $\delta_{0.5}$ in the axial direction. (b) Variation of $(U_e - U_{ctr})/U_e$ in the axial direction. Data are from Liu.¹¹

the fluid kinematic viscosity. Reynolds shear stress is denoted as $R_{uv} = -\langle uv \rangle$, where u and v are the velocity fluctuation in the x - and y - directions, respectively. Angle brackets denote a Reynolds averaging operation. Reynolds normal stress in the x - direction is $R_{uu} = -\langle uu \rangle$ and in the y -direction is $R_{vv} = -\langle vv \rangle$. For a planar turbulent wake flow at sufficiently high Reynolds numbers, the viscous forces and $\partial(R_{uu} - R_{vv})/\partial x$ in the mean momentum equation are typically neglected.²

A. Global integrals of the mean continuity and momentum equations for planar turbulent wakes

The global integral analysis is a powerful tool to uncover the physics of turbulent flows. The first global integral analysis of the mean momentum equation was performed by von Kármán¹⁹ and Pohlhausen²⁰ for wall-bounded turbulent boundary layer flows (see also Ref. 1). The Kármán–Pohlhausen equation presents a relationship among the wall shear stress, free stream velocity, mass deficit thickness, and momentum deficit thicknesses. In the analysis of Kármán and Pohlhausen, the integral of the mean continuity equation was not explicitly presented, but indirectly used in the global integral of the mean momentum equation. In this work, we explicitly derive the global integral of the mean continuity equation.

The global integral of the mean continuity and mean momentum equations, from the wake centerline $y = 0$ to the wake edge δ_e , are (see Subsections 2 and 3 of Appendix A for details) as follows:

$$V_e = \frac{d}{dx} \{ U_e \delta_e - 0.5 \dot{\mathcal{V}} \} - \delta_e \frac{dU_e}{dx}, \quad (2a)$$

$$0 = \frac{d}{dx} \{ 0.5(U_e \dot{\mathcal{V}} - \dot{\mathcal{M}}) \} + \{ U_e \delta_e - 0.5 \dot{\mathcal{V}} \} \frac{dU_e}{dx}, \quad (2b)$$

where $\dot{\mathcal{V}} \stackrel{\text{def}}{=} \int_{-\delta_e}^{\delta_e} U dy$ and $\dot{\mathcal{M}} \stackrel{\text{def}}{=} \int_{-\delta_e}^{\delta_e} U^2 dy$ are the volumetric and the kinematic momentum flow rate over a unit length in the spanwise direction, respectively (see Subsection 1 of Appendix A). Due to symmetry, the mean axial velocity gradient in the transverse direction $\partial U/\partial y$, mean transverse velocity, and Reynolds shear stress are all zero at the wake centerline.

The mean transverse velocity is usually small in wake flows and is difficult to measure accurately. However, Eq. (2a) provides a useful way to estimate the mean transverse velocity at the wake edge, V_e , by using the mean axial velocity profiles measured at multiple axial locations.

Using the definition of I_1 (see Subsection 1 of Appendix A), Eq. (2a) can be expressed as (see Subsection 2 of Appendix A for details)

$$V_e = \frac{d}{dx} [(U_e - U_{ctr}) \delta_e I_1] - \delta_e \frac{dU_e}{dx}. \quad (3)$$

In the wake far fields where the mean axial velocity deficit is observed to reach a self-similar state, I_1 is found to be a constant of $I_1 \approx 0.5$. Equation (3) indicates that the mean transverse velocity at the wake edge V_e can be calculated if U_e , U_{ctr} , δ_e are measured at multiple axial stations. However, to ensure accuracy in the calculation of d/dx , adequate spatial resolution in the axial direction (smaller Δx between the measuring stations) is critical.

Figure 4 shows the variation of the mean transverse velocity, V_e , calculated using Eq. (3) and the curve-fitted values of U_e , $U_e - U_{ctr}$,

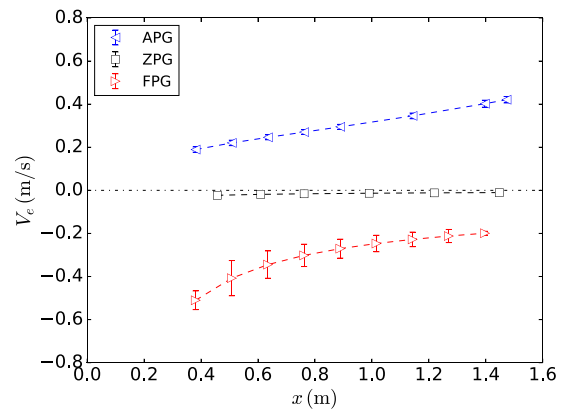


FIG. 4. The mean transverse velocity at the wake edge calculated from Eq. (3). Data are from experimental measurements of Liu.¹¹

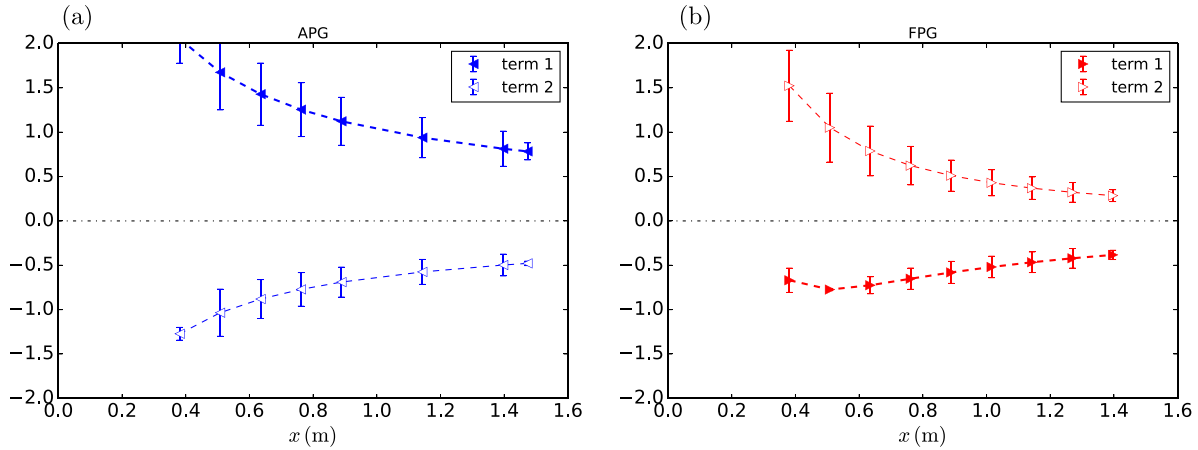


FIG. 5. The first and second terms in the global integral of the mean momentum Eq. (4). The two terms are calculated from the experimental measurements of U_e , U_{ctr} , and δ_e . (a) APG wake. (b) FPG wake. Data are from experimental measurements of Liu.¹¹

and δ_e (see Appendix C for more details on curve fitting). The mean transverse velocity V_e is positive in an APG wake, and the magnitude increases in the axial direction. In a FPG wake, the mean transverse velocity V_e is negative, and its magnitude decreases in the axial direction. In a ZPG wake, V_e is zero in the far field (see Ref. 21). The sign of V_e and its magnitude can provide insight into the nature of the wake flow subjected to APG, ZPG, or FPG. By understanding the variation of V_e under different pressure gradient, researchers can gain a deeper understanding of wake dynamics and use this information to design more efficient fluid systems.

Applying the definitions of I_1 and I_2 , the global integral of the mean momentum Eq. (2b) can be re-written as (see Subsection 3 of Appendix A for details)

$$0 = \underbrace{\frac{d}{dx} [U_e(U_e - U_{ctr})\delta_e I_1 - (U_e - U_{ctr})^2 \delta_e I_2]}_{\text{term1}} + \underbrace{(U_e - U_{ctr})\delta_e I_1 \frac{dU_e}{dx}}_{\text{term2}}. \quad (4)$$

I_2 is defined in Subsection 1 of Appendix A and is found to be a constant of $I_2 \approx 0.36$. To evaluate the validity of the global integral mean momentum Eq. (4), Fig. 5 presents the first and second terms calculated using the curved-fitted δ_{05} , U_e , and $U_e - U_{ctr}$ for the APG and FPG wakes. In an APG wake, U_e decreases in the axial direction and the second term in Eq. (4) is negative. In contrast, in a FPG wake, U_e increases in the axial direction and the second term in Eq. (4) is positive, as shown in Fig. 5(b). Overall, the two terms shown in Fig. 5 exhibit similar magnitude and opposite signs in the far wake, as dictated by the global integral constraint Eq. (4).

Figure 3(b) shows that in the far field of ZPG or FPG wakes, the maximum axial velocity deficit becomes much smaller than the free stream velocity: $U_e - U_{ctr} \ll U_e$. Thus, the $(U_e - U_{ctr})^2$ term in Eq. (4) is negligible, and the global integral of the mean momentum Eq. (4) can be approximated as

$$\frac{d}{dx} [U_e(U_e - U_{ctr})\delta_e I_1] \approx -(U_e - U_{ctr})\delta_e I_1 \frac{dU_e}{dx}. \quad (5)$$

This equation can be rearranged as

$$\frac{1}{U_e(U_e - U_{ctr})\delta_e I_1} \frac{d[U_e(U_e - U_{ctr})\delta_e I_1]}{dx} \approx -\frac{1}{U_e} \frac{dU_e}{dx}. \quad (6)$$

Simple integration gives a relation among U_e , $(U_e - U_{ctr})$, and δ_e :

$$U_e^2 (U_e - U_{ctr}) \delta_e = \text{const.} \quad \text{if } (U_e - U_{ctr}) \ll U_e. \quad (7)$$

This relation can be obtained from a self-similarity analysis and was reported by a number of researchers, e.g., Townsend (Eq. 6.4.12 in Ref. 2), Narasimha and Prabhu,⁹ and Liu *et al.*^{11,12} For a planar wake flow under ZPG, U_e is a constant and Eq. (7) can be further simplified as

$$(U_e - U_{ctr}) \delta_e = \text{const.} \quad \text{ZPG wake.} \quad (8)$$

This relation has been presented routinely in previous studies of planar turbulent wakes under ZPG, such as Refs. 9,12, and 21.

B. Maximum Reynolds shear stress from integral analysis

Empirically, it is observed that the normalized Reynolds shear stress profiles reach a self-similar shape away from the wake generator, and the maximum Reynolds shear stress is located at $y_m \approx 0.84\delta_{0.5}$ (see Fig. 17). Hence, an equation for the maximum Reynolds shear stress can be obtained by integrating the mean momentum equation from the wake centerline to y_m as (the steps are similar to the global integral in Subsection 2 and 3 of Appendix A),

$$R_{uv}|_{\max} = \frac{d}{dx} \left\{ U_e^2 y_m - 2U_e(U_e - U_{ctr})y_m I_{1m} + (U_e - U_{ctr})^2 y_m I_{2m} \right\} - U_{y_m} \frac{d}{dx} \left\{ U_e y_m - (U_e - U_{ctr})y_m I_{1m} \right\} - y_m U_e \frac{dU_e}{dx}, \quad (9)$$

where $I_{1m} \approx 0.86$ and $I_{2m} \approx 0.76$ (see Subsection 1 of Appendix A). While Eq. (9) appears complex, the only measurement required is the mean axial velocity at multiple axial stations. All the variables on the right side of Eq. (9), U_e , $U_e - U_{ctr}$, y_m , I_{1m} , and I_{2m} , are obtained from the mean axial velocity profiles.

Figure 6 compares the measured maximum Reynolds shear stress $R_{uv}|_{\max}$ with the analytical prediction from the integral Eq. (9). The

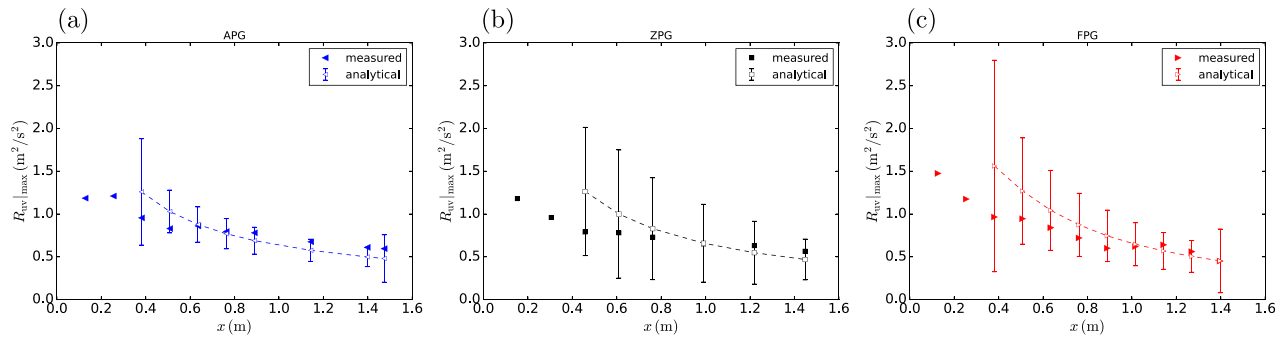


FIG. 6. Maximum Reynolds shear stress from experimental measurements and analytical Eq. (9): (a) APG wake, (b) ZPG wake, and (c) FPG wake. Data are from experimental measurements of Liu.¹¹

agreement between the analytical prediction and the measured values in Fig. 6 supports the validity of the integral equation (9) for predicting the maximum Reynolds shear stress.

IV. SELF-SIMILARITY SOLUTIONS OF PLANAR TURBULENT WAKES UNDER PRESSURE GRADIENT

Figure 3 shows that the wake half-width $\delta_{0.5}$ and the mean maximum axial velocity deficit $U_e - U_{ctr}$ are strongly affected by the pressure gradients. However, it is known that shapes of the mean axial velocity deficit profiles become self-similar in the far field.^{2,11} As shown in Fig. 7, the normalized profiles of $(U_e - U)/(U_e - U_{ctr})$ collapse onto a single curve in the far field of planar turbulent wakes, when plotted against $y/\delta_{0.5}$, regardless of the pressure gradient. The self-similar function for the mean axial velocity deficit can be approximated as

$$U^* = \frac{U_e - U}{U_e - U_{ctr}} \approx e^{(-0.637\eta^2 - 0.056\eta^4)}, \tag{10}$$

where $\eta = y/\delta_{0.5}$ is the transverse location normalized by the wake's half-width. This approximation function has been used by Wygnanski *et al.*²² and Liu.¹¹

Liu *et al.*¹² found that a universal shape for U^* is established in planar turbulent wakes subjected to ZPG, APG, or FPG when $x/\theta_0 > 40$, where θ_0 is the initial wake momentum thickness. Thus $x/\theta_0 \approx 40$ can be used as the delimiter of the far wake. The self-similar shape implies that the mean axial velocity deficit profiles can

be characterized by one length scale $\delta_{0.5}$ and one velocity scale $U_e - U_{ctr}$. Note that in Fig. 7, the U^* profiles at the near wake stations of $x = 5$ or 6 in. ($x/\theta_0 = 17.6$ or 21.1) are still developing and have not reached the self-similar state yet.

Given the direct connections among the mean axial flow, the mean transverse flow, and Reynolds shear stress in the mean momentum equation, rational questions arise: Far from the wake generator, do the mean transverse flow V and Reynolds shear stress R_{uv} also approach a self-similar state? If profiles of V or R_{uv} do not reach a self-similar state, then additional length scales would be required to describe the profiles of V or R_{uv} . How would the additional length scales be related to the single length scale for the U^* profile? If the profiles of V or R_{uv} approach a self-similar state, then their proper scales need to be determined. Determining the proper scales for the mean transverse flow and the Reynolds shear stress is an important step in fully characterizing the flow and understanding the underlying physics.

A. Analytical and approximate equations for the mean transverse velocity

The mean transverse velocity is a key parameter that provides information about the transverse flow structure in the wake and its evolution in the axial direction. An analytical equation for the mean transverse velocity can be obtained by integrating the mean continuity Eq. (1a) from 0 (wake centerline) to y ,

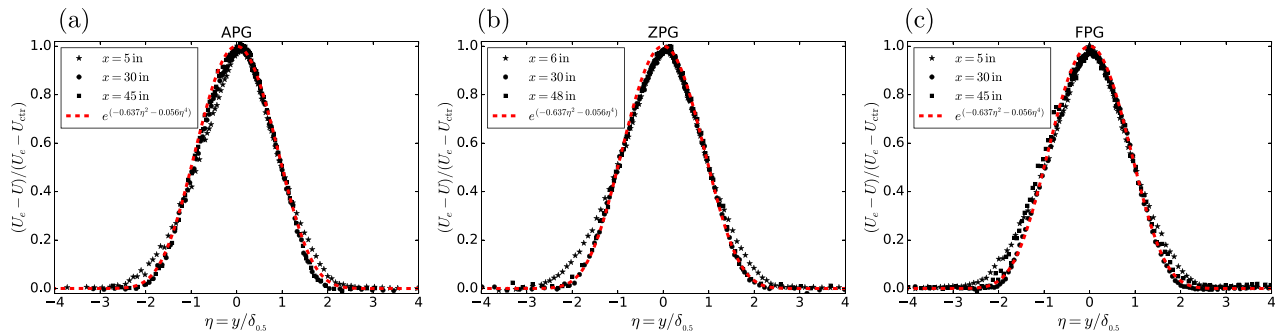


FIG. 7. Normalized mean velocity deficit profiles in planar turbulent wakes under pressure gradients: (a) APG wake, (b) ZPG wake, and (c) FPG wake. The dashed curve is the approximation Eq. (10). Data are from experimental measurements of Liu.¹¹

$$V = - \int_0^y \frac{\partial U}{\partial x} dy = - \frac{dU_e}{dx} y + \int_0^y \frac{\partial(U_e - U)}{\partial x} dy. \quad (11)$$

Applying the self-similarity assumption of $U^* = f(\eta)$, the x -derivative of the mean axial velocity deficit can be written as

$$\frac{\partial(U_e - U)}{\partial x} = \frac{d(U_e - U_{ctr})}{dx} U^* - \frac{(U_e - U_{ctr})}{\delta_{0.5}} \frac{d\delta_{0.5}}{dx} \eta \frac{dU^*}{d\eta}. \quad (12)$$

The integral of $\partial(U_e - U)/\partial x$ then becomes

$$\begin{aligned} \int_0^y \frac{\partial(U_e - U)}{\partial x} dy &= \int_0^\eta \frac{d(U_e - U_{ctr})}{dx} U^* \delta_{0.5} d\eta \\ &\quad - \int_0^\eta \frac{(U_e - U_{ctr})}{\delta_{0.5}} \frac{d\delta_{0.5}}{dx} \eta \frac{dU^*}{d\eta} \delta_{0.5} d\eta \\ &= \frac{d((U_e - U_{ctr})\delta_{0.5})}{dx} \int_0^\eta U^* d\eta \\ &\quad - (U_e - U_{ctr}) \frac{d\delta_{0.5}}{dx} \eta U^*. \end{aligned} \quad (13)$$

Substituting Eq. (13) into Eq. (11) gives an analytical equation for the mean transverse velocity as

$$\begin{aligned} V &= - \underbrace{\delta_{0.5} \frac{dU_e}{dx}}_{a_I} \eta \\ &\quad + \underbrace{\frac{d((U_e - U_{ctr})\delta_{0.5})}{dx}}_{a_{II}} \int_0^\eta U^* d\eta - \underbrace{(U_e - U_{ctr}) \frac{d\delta_{0.5}}{dx}}_{a_{III}} \eta U^*. \end{aligned} \quad (14)$$

Note that each of the three pre-factors $a_I = -\delta_{0.5} dU_e/dx$, $a_{II} = d[(U_e - U_{ctr})\delta_{0.5}]/dx$, or $a_{III} = -(U_e - U_{ctr})d\delta_{0.5}/dx$ is a velocity scale. Hence, the mean transverse flow in planar turbulent wakes under pressure gradient consists of three components, each associated with a distinct velocity scale. Equation (14) provides a useful framework for understanding the mean transverse flow in planar turbulent wakes under pressure gradient and how it is related to different velocity scales.

In a ZPG wake, $U_e = \text{const}$ and $(U_e - U_{ctr})\delta_{0.5} = \text{const}$, so $a_I = a_{II} = 0$. Consequently, the mean transverse velocity Eq. (14) can be simplified for a ZPG wake as

$$V = -(U_e - U_{ctr}) \frac{d\delta_{0.5}}{dx} \eta U^*, \quad \text{ZPG wake} \quad (15)$$

consistent with the result reported in Ref. 21

For simplicity, U^* is approximated by a Gaussian function $U^* \approx \exp(-a\eta^2)$, where $a = \ln(2)$. The difference between this simple Gaussian function and Eq. (10) is minor and limited to the wake edge region (see Ref. 21). Then, an approximate equation for the mean transverse velocity can be obtained from Eq. (14) as

$$\begin{aligned} V &= -\delta_{0.5} \frac{dU_e}{dx} \eta + \frac{d[(U_e - U_{ctr})\delta_{0.5}]}{dx} \frac{\sqrt{\pi}}{2\sqrt{a}} \text{erf}(\sqrt{a}\eta) \\ &\quad - (U_e - U_{ctr}) \frac{d\delta_{0.5}}{dx} \eta \exp(-a\eta^2). \end{aligned} \quad (16)$$

Using hot wire measurements, Liu¹¹ determined the mean transverse velocity profiles at the axial location of $x/\theta_0 = 141$. The relevant

TABLE I. Parameters in Eq. (16). The parameters are for $x/\theta_0 = 141$ or $x = 1.01$ m.

	APG wake	ZPG wake	FPG wake
$\delta_{0.5}$ (mm)	25	22	17.8
$a_I = -\delta_{0.5} dU_e/dx$ (m/s)	0.125	0	-0.125
$a_{II} = d[(U_e - U_{ctr})\delta_{0.5}]/dx$ (m/s)	0.07	0	-0.05
$a_{III} = -(U_e - U_{ctr})d\delta_{0.5}/dx$ (m/s)	-0.12	-0.06	-0.02

parameters at this location, determined from the measurement of U distribution, are listed in Table 1. Applying the parameters in Table 1, the mean transverse velocity profiles are calculated using the approximate Eq. (16), and compared with the experimentally measured V in Fig. 8, showing excellent agreement.

In general, the mean transverse velocity Eq. (16) consists of three self-similar functions: η , $\text{erf}(\sqrt{a}\eta)$, and $\eta \exp(-a\eta^2)$. The shapes of the three functions are shown in Fig. 9. The first term of Eq. (16), $-\delta_{0.5} dU_e/dx \eta = -y dU_e/dx = y \partial V/\partial y|_e$, is a linear function of y , representing the mean transverse flow in the free stream imposed by the pressure gradient. The last term is similar to the mean transverse flow in a ZPG wake (see Ref. 21).

Figure 10 presents the variations of pre-factors a_I , a_{II} , and a_{III} in Eq. (14). In the far field, a_I is zero in a ZPG wake, and is positive (negative) in an APG (FPG) wake. The magnitude of a_I increases in the axial direction of the APG wake, but decreases in the FPG wake. Figure 10(b) shows that a_{II} is zero in the far field of a ZPG wake, which confirms the constraint reported in Ref. 21. In an APG wake, the deficit $(U_e - U_{ctr})$ decreases slowly in the axial direction, but $\delta_{0.5}$ increases more rapidly (see Fig. 3). Therefore, the magnitude of the product $(U_e - U_{ctr})\delta_{0.5}$ increases in the axial direction of an APG wake, and a_{II} is positive as shown in Fig. 10(b). On the other hand, the magnitude of the product $(U_e - U_{ctr})\delta_{0.5}$ decreases in the axial direction of FPG wakes, and a_{II} is negative. Figure 10(c) shows that the pre-factor a_{III} is negative in all the three wakes.

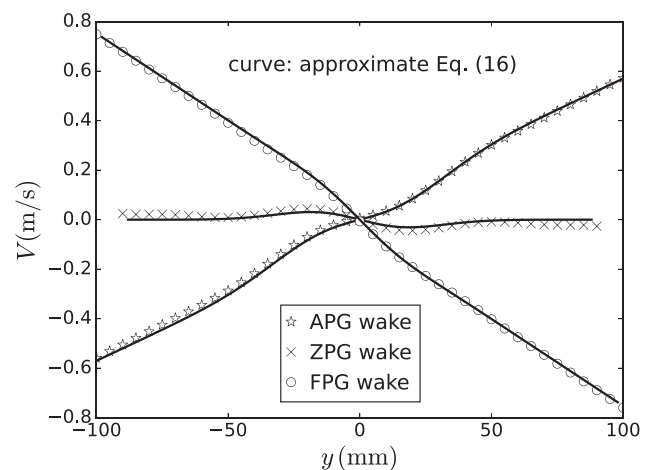


FIG. 8. Comparison of approximate Eq. (16) for V with experimental measurements. The data of Liu¹¹ were measured at $x/\theta_0 = 141$ or $x = 1.015$ m. To prevent clutter, every 5th measurement of V is plotted.

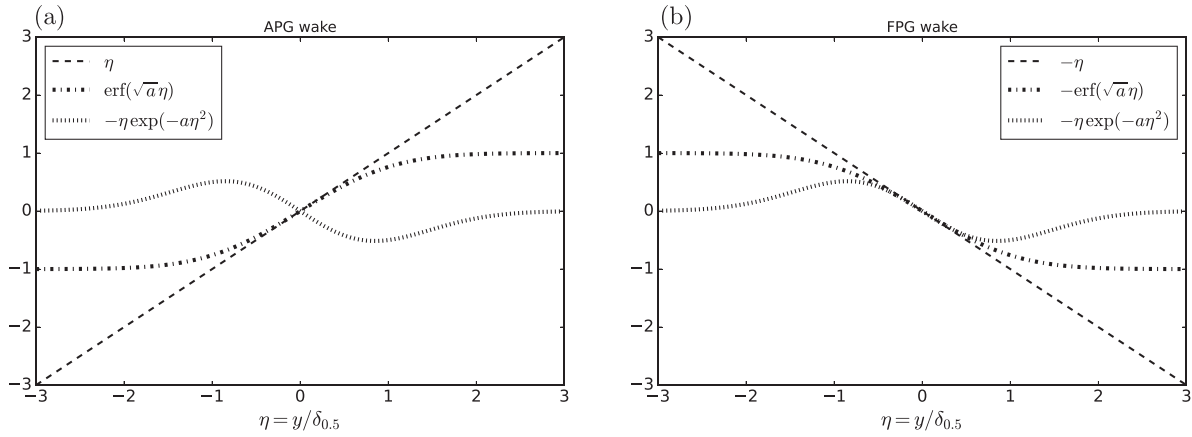


FIG. 9. Components of mean transverse flow in planar turbulent wakes under pressure gradient. (a) APG wake. (b) FPG wake.

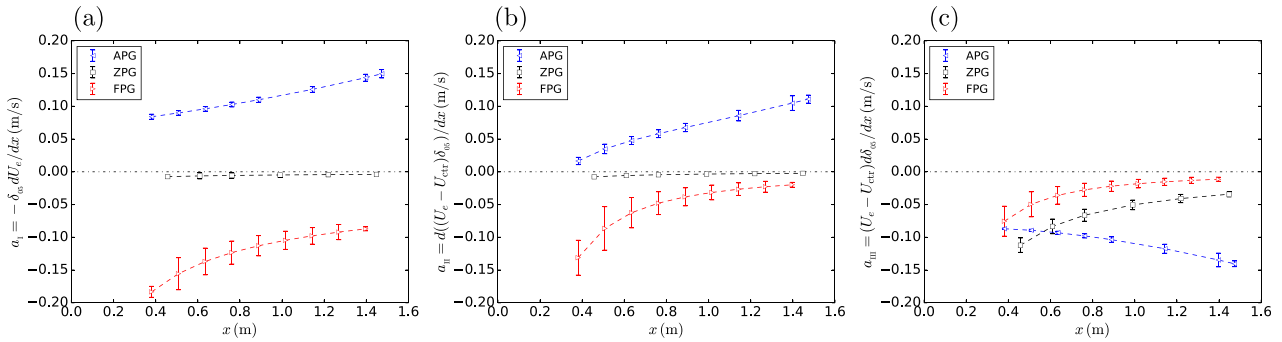


FIG. 10. Pre-factors of terms in the mean transverse velocity Eq. (14): (a) $a_I = -\delta_{0.5} dU_e/dx$ vs x ; (b) $a_{II} = d((U_e - U_{ctr})\delta_{0.5})/dx$ vs x ; and (c) $a_{III} = -(U_e - U_{ctr})d\delta_{0.5}/dx$ vs x .

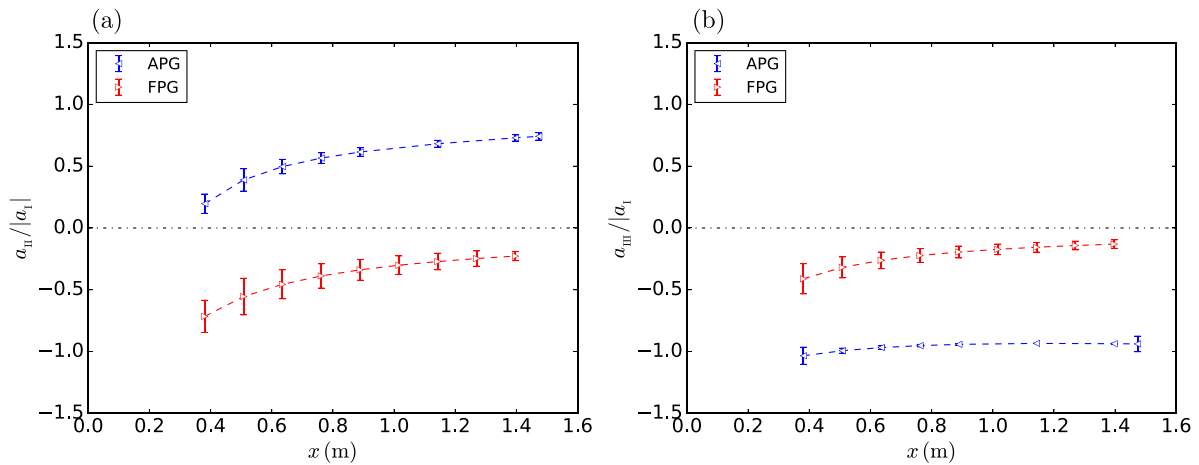


FIG. 11. (a) Ratio of $a_{II}/|a_I|$ vs x . (b) Ratio of $a_{III}/|a_I|$ vs x .

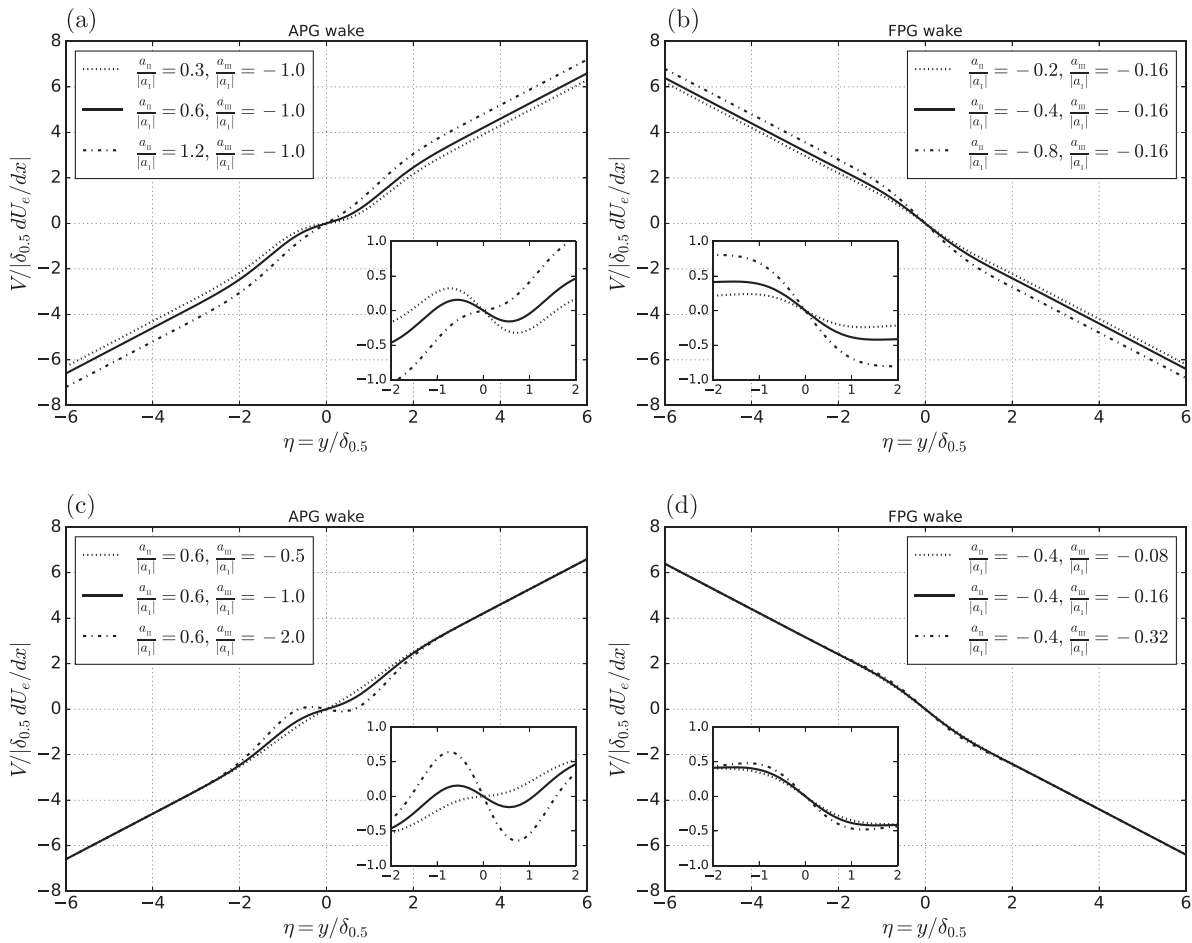


FIG. 12. Mean transverse velocity normalized by $|a_I|$ (or $|\delta_{0.5} dU_e/dx|$). Effects of $a_{II}/|a_I|$ and $a_{III}/|a_I|$: (a) APG wake with different $a_{II}/|a_I|$; (b) FPG wake with different $a_{II}/|a_I|$; (c) APG wake with different $a_{III}/|a_I|$; and (d) FPG wake with different $a_{III}/|a_I|$. The insets show the sum of the last two terms in Eq. (17) (without the linear function).

At the wake edge $y = \delta_e$ or $\eta_e = \delta_e/\delta_{0.5}$, the last term in Eq. (14) or Eq. (16) is close to zero as shown in Fig. 9. Therefore, Eq. (14) at $y = \delta_e$ reproduces the global integral result Eq. (3): $V_e - \delta_e \partial V/\partial y|_e = a_{II} \eta_e I_1$. Figure 10 shows that a_{II} is not zero for an APG or FPG wake. Hence, Eq. (14) indicates that the mean transverse velocity at the edge of APG or FPG wakes is not $\delta_e \partial V/\partial y|_e$. In other words, the mean transverse velocity in the free stream is tilted from the linear function $y \partial V/\partial y|_e$ by the second term in Eq. (14) or Eq. (16) (see Figs. 8 and 12).

In any wake flow, the parameters a_I , a_{II} , and a_{III} can be obtained by measuring the U profiles at multiple axial locations. Once a_I , a_{II} , and a_{III} are determined from experimental or numerical data, Eq. (16) can be used to calculate the mean transverse velocity at that location. To understand the effect of a_I , a_{II} , and a_{III} on the shape of V , it is better to present the mean transverse velocity profile in a dimensionless form, which can be obtained by dividing Eq. (16) by one of the velocity scales, a_I , a_{II} , or a_{III} . For example, dividing Eq. (16) by $|\delta_{0.5} dU_e/dx|$ gives a dimensionless equation for the mean transverse velocity as

$$\frac{V}{|\delta_{0.5} \frac{dU_e}{dx}|} = \underbrace{\frac{-\delta_{0.5}}{|\delta_{0.5} \frac{dU_e}{dx}|}}_{a_I/|a_I|} \eta + \frac{d[(U_e - U_{ctr})\delta_{0.5}]}{dx} \underbrace{\frac{\sqrt{\pi}}{2\sqrt{a}} \operatorname{erf}(\sqrt{a}\eta)}_{a_{II}/|a_I|} + \underbrace{\frac{-(U_e - U_{ctr}) \frac{d\delta_{0.5}}{dx}}{|\delta_{0.5} \frac{dU_e}{dx}|}}_{a_{III}/|a_I|} \eta \exp(-a\eta^2). \quad (17)$$

The shape of the normalized mean transverse velocity Eq. (17) depends on the two ratios $a_{II}/|a_I|$ and $a_{III}/|a_I|$, which are shown in Fig. 11. The ratio $a_{II}/|a_I|$ is positive for the APG wake, but is negative for the FPG wake. The ratio $a_{III}/|a_I|$ is negative for both the APG and FPG wakes. As shown in Fig. 3(a), $\delta_{0.5}$ of the APG wake increases much faster than that of the FPG wake. Therefore, the magnitude of the ratio $a_{III}/|a_I|$ in the APG wake is larger than that of the FPG wake.

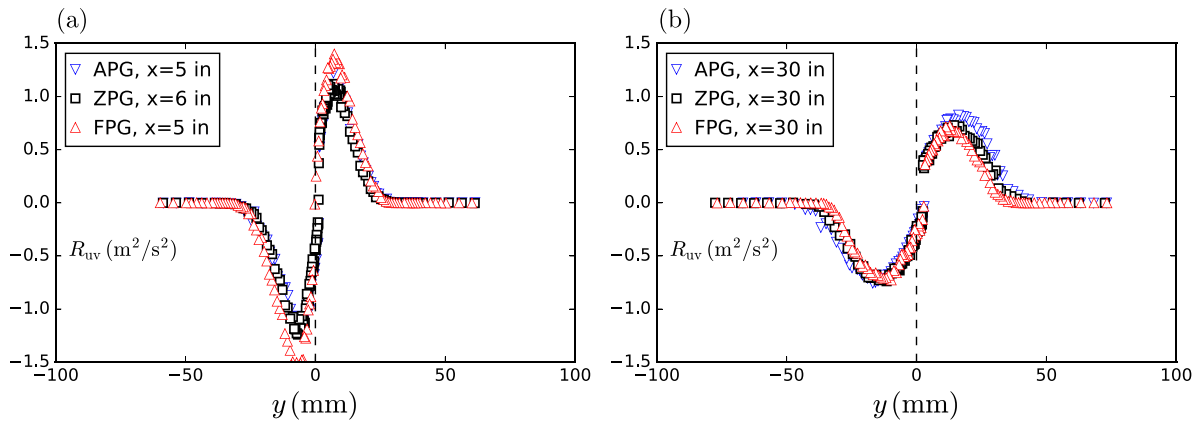


FIG. 13. Typical evolution of Reynolds shear stress profiles in planar turbulent wake flow under APG, ZPG, and FPG: (a) At a near wake location and (b) At $x = 30$ in. Data are from experimental measurements of Liu.¹¹

Figure 11 shows that the ratios $a_{II}/|a_I|$ and $a_{III}/|a_I|$ approach constant values in the far field. In other words, the normalized mean transverse velocity Eq. (17) become self-similar far from the wake initiator. However, the ratios $a_{II}/|a_I|$ and $a_{III}/|a_I|$ are not universal, but depend on the pressure gradient. For example, with increasing pressure gradient, the pre-factor a_I in an APG or FPG wake becomes larger, and the ratio of $a_{III}/|a_I|$ will become smaller. On the other hands, as the pressure gradient decreases toward zero, the pre-factor a_I in an APG or FPG wake also decreases toward zero, and the ratio $a_{III}/|a_I|$ will become larger.

The effect of pressure gradients on the shape of the mean transverse flow are illustrated here using Eq. (17) with different values of $a_{II}/|a_I|$ and $a_{III}/|a_I|$. Figure 12(a) shows the effects of $a_{II}/|a_I|$ on the shape of the mean transverse velocity in the APG wake. The inset presents the sum of the last two terms in Eq. (17), showing the effects of $a_{II}/|a_I|$ on the mean transverse flow inside the wake. In Fig. 12(a), the ratio $a_{III}/|a_I| = -1$ is kept the same as that in Table 1, and three values of $a_{II}/|a_I| = 0.3, 0.6,$ and 1.2 are used. The solid black curve with $a_{II}/|a_I| = 0.6$ corresponds to the experimental data of Liu.¹¹ As $a_{II}/|a_I|$ increases, the tilt from the linear function $y\partial V/\partial y|_e$ becomes larger, and the transverse flow within the wake deviates more from the shape in the ZPG wake.

Figure 12(b) presents the shapes of the mean transverse velocity in the FPG wake at three values of $a_{II}/|a_I| = -0.2, -0.4,$ and -0.8 . The ratio $a_{III}/|a_I|$ is kept at -0.16 . The solid black curve corresponds to the data in Table 1. Similar to the APG wake, the increase in the magnitude of $a_{II}/|a_I|$ results in a larger tilt of the mean transverse flow from the $y\partial V/\partial y|_e$ curve.

Figure 12(c) presents the effect of $a_{III}/|a_I|$ on the shape of the mean transverse flow in the APG wake, and the inset shows the sum of the last two terms in Eq. (17). The ratio $a_{II}/|a_I|$ is kept at 0.6 , and three values of $a_{III}/|a_I|$ are $-0.5, -1.0,$ and -2.0 . The tilt of the mean transverse flow from the linear function $y\partial V/\partial y|_e$ is fixed in Fig. 12(c), but the transverse flow inside the wake is stronger for the larger magnitude of $a_{III}/|a_I|$. Figure 12(d) presents the effect of $a_{III}/|a_I|$ on the shape of the mean transverse flow in the FPG wake. At a fixed value of $a_{II}/|a_I| = -0.4$, the influence of three values of $a_{III}/|a_I| = -0.08, -0.16, -0.32$ is minor on the shape of the mean transverse velocity.

As pressure gradient approaches zero, the pre-factor $a_I = \delta_{0.5}dU_e/dx$ also approaches zero and the curves in Fig. 12 become unbounded. In order to better illustrate the effect of pressure gradient on the mean transverse velocity under small pressure gradient, one can normalize Eq. (16) by either a_{II} or a_{III} . The profiles of the mean transverse velocity normalized by $|U_e - U_{ctr}|d\delta_{0.5}/dx|$ are presented in Appendix B. This information can be useful in understanding how the pressure gradient influences the mean transverse velocity, as well as how to present the velocity data in a way that makes it easier to interpret the effect of pressure gradient.

B. Analytical and approximate equations for the Reynolds shear stress

Reynolds shear stress is one of the most important quantities in the analysis and modeling of turbulent wake flow. Figure 13(a) shows that the Reynolds shear stress profiles in a near wake location are similar for the APG, ZPG, and FPG wakes. Figure 13(b) shows that, at a downstream location of $x = 30$ in., the shapes of the Reynolds shear stress profiles under different pressure gradients are still similar, but the width and the magnitude are affected by the pressure gradients.

In previous studies, there has been a lack of agreement on how to properly scale the Reynolds shear stress. The Reynolds shear stress profiles normalized by the traditional scale $(U_e - U_{ctr})^2$ fail to capture the self-similarity.^{12,23} Alternative scale has been proposed to provide a more accurate characterization of the self-similarity of the normalized Reynolds shear stress, by accounting for the axial variation of the wake width and free stream velocity.^{11,14} Here, a self-similarity analysis of the mean momentum equation rigorously reveals a more complete understanding of the Reynolds shear stress by decomposing it into four distinct components, each of which is associated with a different scale. This result provides a new framework for understanding the Reynolds shear stress and its role in the turbulent wake flow.

An analytical equation for the Reynolds shear stress can be obtained by integrating the mean momentum Eq. (1b) from the wake centerline to y , utilizing the mean continuity Eq. (1a), and applying boundary conditions,

$$0 = - \int_0^y \frac{\partial U^2}{\partial x} dy - (UV - 0) - \int_0^y \frac{1}{\rho} \frac{dP_\infty}{dx} dy + (R_{uv} - 0). \quad (18)$$

To apply the self-similarity assumption, the mean axial velocity in Eq. (18) is rearranged as $U_e - (U_e - U)$, and the Reynolds shear stress can be written as

$$\begin{aligned} R_{uv} &= -(U_e - U)V + U_e V - U_e \frac{dU_e}{dx} y + \int_0^y \frac{\partial(U_e - U - U_e)^2}{\partial x} dy \\ &= -(U_e - U)V + U_e V - U_e \frac{dU_e}{dx} y + \int_0^y \frac{\partial(U_e - U)^2}{\partial x} dy \\ &\quad - 2U_e \int_0^y \frac{\partial(U_e - U)}{\partial x} dy - 2 \frac{dU_e}{dx} \int_0^y (U_e - U) dy + 2U_e \frac{dU_e}{dx} y. \end{aligned} \quad (19)$$

Substituting V in Eq. (11) into Eq. (19), the Reynolds shear stress can be presented as

$$\begin{aligned} R_{uv} &= -U_e \int_0^y \frac{\partial(U_e - U)}{\partial x} dy - 2 \frac{dU_e}{dx} \int_0^y (U_e - U) dy \\ &\quad + (U_e - U) \left(\frac{dU_e}{dx} y - \int_0^y \frac{\partial(U_e - U)}{\partial x} dy \right) + \int_0^y \frac{\partial(U_e - U)^2}{\partial x} dy. \end{aligned} \quad (20)$$

Assuming self-similarity for U^* , the term $\partial(U_e - U)^2/\partial x$ can be written as

$$\begin{aligned} \frac{\partial(U_e - U)^2}{\partial x} &= 2(U_e - U_{ctr}) \frac{d(U_e - U_{ctr})}{dx} (U^*)^2 \\ &\quad - 2 \frac{(U_e - U_{ctr})^2}{\delta_{0.5}} \frac{d\delta_{0.5}}{dx} \eta U^* \frac{dU^*}{d\eta} \\ &= \frac{1}{\delta_{0.5}} \frac{d((U_e - U_{ctr})^2 \delta_{0.5})}{dx} (U^*)^2 \\ &\quad - \frac{(U_e - U_{ctr})^2}{\delta_{0.5}} \frac{d\delta_{0.5}}{dx} \frac{d(\eta(U^*)^2)}{d\eta}. \end{aligned} \quad (21)$$

The integral of Eq. (21) is

$$\begin{aligned} \int_0^y \frac{\partial(U_e - U)^2}{\partial x} dy &= \frac{d((U_e - U_{ctr})^2 \delta_{0.5})}{dx} \int_0^\eta (U^*)^2 d\eta \\ &\quad - (U_e - U_{ctr})^2 \frac{d\delta_{0.5}}{dx} \eta (U^*)^2. \end{aligned} \quad (22)$$

The integral of $(U_e - U)$ is

$$\int_0^y (U_e - U) dy = \delta_{0.5} (U_e - U_{ctr}) \int_0^\eta U^* d\eta. \quad (23)$$

Substituting Eqs. (13), (22), and (23) into Eq. (20) yields a new analytical equation for the Reynolds shear stress as

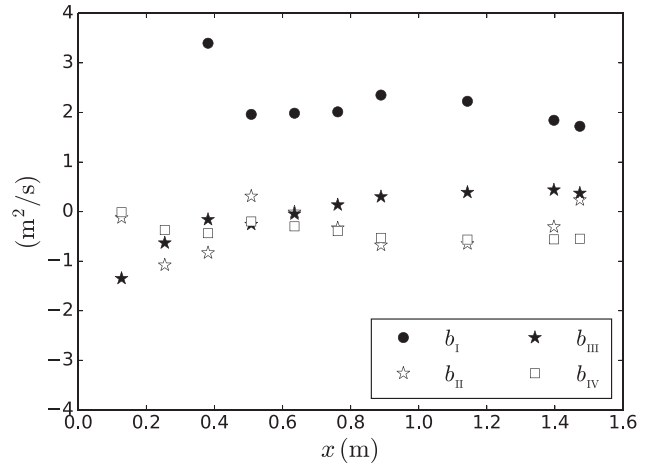


FIG. 14. Pre-factors of terms in the R_{uv} Eq. (24) for the APG wake case of Liu's experiment.¹¹

$$\begin{aligned} R_{uv} &= \underbrace{(U_e - U_{ctr}) \frac{d(U_e \delta_{0.5})}{dx}}_{b_I} \eta U^* \\ &\quad - \underbrace{\left[\frac{d(U_e (U_e - U_{ctr}) \delta_{0.5})}{dx} + (U_e - U_{ctr}) \delta_{0.5} \frac{dU_e}{dx} \right]}_{b_{II}} \int_0^\eta U^* d\eta \\ &\quad + \underbrace{\frac{d((U_e - U_{ctr})^2 \delta_{0.5})}{dx}}_{b_{III}} \int_0^\eta (U^*)^2 d\eta \\ &\quad - \underbrace{(U_e - U_{ctr}) \frac{d((U_e - U_{ctr}) \delta_{0.5})}{dx}}_{b_{IV}} U^* \int_0^\eta U^* d\eta. \end{aligned} \quad (24)$$

Equation (24) indicates that the Reynolds shear stress in planar turbulent wakes consists of four components, each associated with its own scale b_I , b_{II} , b_{III} , and b_{IV} . Figure 3(b) shows that in the far field of ZPG or FPG wakes, $U_e - U_{ctr} \ll U_e$. Consequently, the pre-factor b_{II} in Eq. (24) approaches zero in the far field of ZPG or FPG wakes [see Eq. (5)]. The pre-factors b_{III} and b_{IV} are proportional to $(U_e - U_{ctr})^2$ and are much smaller than b_I in the far fields of ZPG or FPG wakes. Figure 14 presents the variations of b_I , b_{II} , b_{III} , and b_{IV} in an APG wake, showing that b_I has the largest magnitude.

The four self-similar functions in Eq. (24) can be simplified by employing the approximation of $U^* \approx \exp(-a\eta^2)$:

$$\eta U^* \approx \eta \exp(-a\eta^2), \quad (25a)$$

$$\int_0^\eta U^* d\eta \approx \sqrt{\pi/(4a)} \operatorname{erf}(\sqrt{a}\eta), \quad (25b)$$

$$\int_0^\eta (U^*)^2 d\eta \approx \sqrt{\pi/(8a)} \operatorname{erf}(\sqrt{2a}\eta), \quad (25c)$$

$$U^* \int_0^\eta U^* d\eta \approx \sqrt{\pi/(4a)} \operatorname{erf}(\sqrt{a}\eta) \exp(-a\eta^2). \quad (25d)$$

The shapes of the four self-similar functions in Eqs. (25a)–(25d) are illustrated in Fig. 15. Outside the wake, Eqs. (25a) and (25d) approach

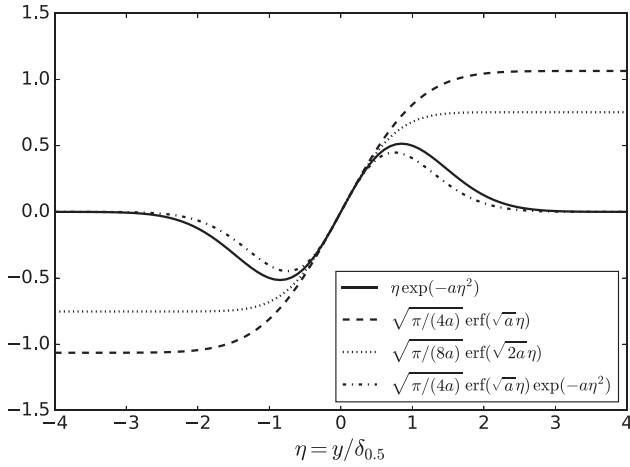


FIG. 15. The four self-similar functions for the R_{uv} Eq. (24).

zero, but Eqs. (25b) and (25c) do not. As the Reynolds shear stress becomes zero outside the wake, the pre-factors b_{II} and b_{III} must have opposite signs and $b_{II} \approx -\sqrt{2} b_{III}$ in order to cancel their contributions in the free stream, as shown in Fig. 14.

In the far fields of APG, ZPG, or FPG wakes, the dominant component in Eq. (24) is the first term, and the Reynolds shear stress can be approximated as

$$R_{uv} \approx (U_e - U_{ctr}) \frac{d(U_e \delta_{0.5})}{dx} \eta U^* \quad \text{wake far field} \quad (26)$$

Equation (26) indicates that a proper scale for the Reynolds shear stress in planar turbulent wakes under pressure gradient is $R_{uv,ref} = (U_e - U_{ctr})d(U_e \delta_{0.5})/dx$. This scale has been reported by Liu¹¹ and Thomas and Liu.¹⁴ In the far field of a ZPG wake where $U_e = \text{const}$, Eq. (26) becomes

$$R_{uv} \approx U_e(U_e - U_{ctr}) \frac{d\delta_{0.5}}{dx} \eta U^*, \quad \text{ZPG wake} \quad (27)$$

consistent with the result presented in Ref. 21. In a ZPG wake, the proper scale for the Reynolds shear stress is $U_e V_{ref}$, where $V_{ref} = (U_e - U_{ctr})d\delta_{0.5}/dx$.

By substituting Eq. (10) for U^* into Eq. (26), we can determine that the maximum Reynolds shear stress occurs at $\eta \approx 0.84$, with a maximum value of $R_{uv,max} \approx 0.52(U_e - U_{ctr})d(U_e \delta_{0.5})/dx$. Figure 16 illustrates a comparison between the measured maximum Reynolds shear stress and the calculated value of $(U_e - U_{ctr})d(U_e \delta_{0.5})/dx$. The figure demonstrates that the variation in the measured $R_{uv,max}$ data aligns with the trend of the calculated values of $0.52(U_e - U_{ctr})d(U_e \delta_{0.5})/dx$, with the scatter primarily attributed to

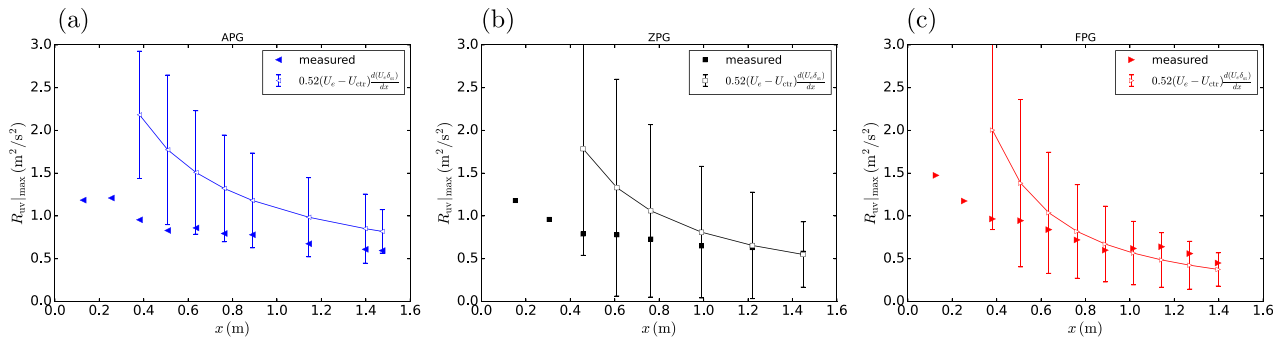


FIG. 16. Comparison of the Reynolds shear stress scale $(U_e - U_{ctr})d(U_e \delta_{0.5})/dx$ with the maximum Reynolds shear stress. Note that the reference scale is multiplied by a factor of 0.52: (a) APG wake, (b) ZPG wake, and (c) FPG wake. Data are from experimental measurements of Liu.¹¹

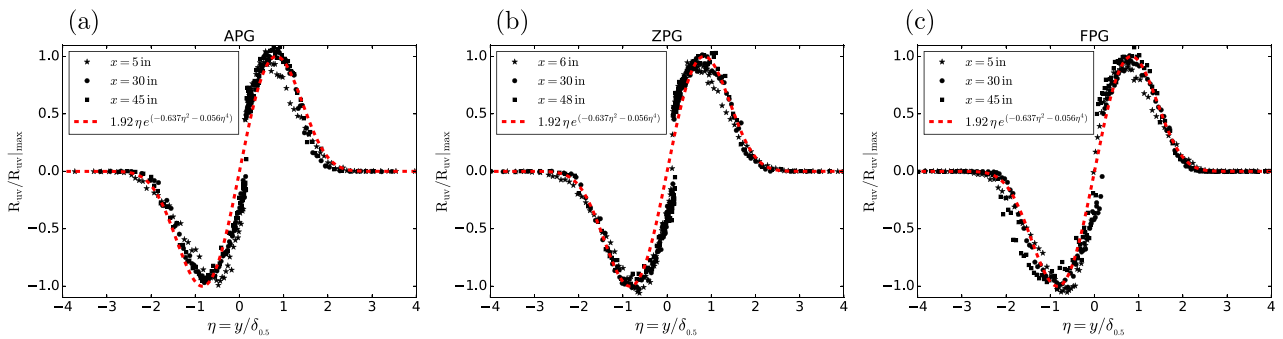


FIG. 17. Reynolds shear stress normalized by its maximum value: (a) APG wake, (b) ZPG wake, and (c) FPG wake. Data are from experimental measurements of Liu.¹¹

TABLE II. Major results from the analyses of planar turbulent wakes under pressure gradient.

Global integral of mean continuity equation	$V_e = \frac{d}{dx} \{ U_e \delta_e - 0.5 \dot{\gamma} \} - \delta_e \frac{dU_e}{dx}$
Global integral of mean momentum equation	$0 = \frac{d}{dx} \{ 0.5(U_e \dot{\gamma} - \dot{M}) \} + \{ U_e \delta_e - 0.5 \dot{\gamma} \} \frac{dU_e}{dx}$
Analytical equation for maximum R_{uv}	Eq. (9)
Approximate relation for shallow wakes	$U_e^2 (U_e - U_{ctr}) \delta_e = \text{const.}$
Empirical equation for Reynolds shear stress	$\frac{R_{uv}}{ R_{uv} _{\max}} \approx 1.92\eta e^{(-0.637\eta^2 - 0.056\eta^4)} = 1.92\eta U^*$
Analytical mean transverse velocity	$V = -\delta_{0.5} \frac{dU_e}{dx} \eta + \frac{d((U_e - U_{ctr})\delta_{0.5})}{dx} \int_0^\eta U^* d\eta - (U_e - U_{ctr}) \frac{d\delta_{0.5}}{dx} \eta U^*$
Analytical Reynolds shear stress	Eq. (24)

the uncertainty in calculating the x -derivative component of $d(U_e \delta_{0.5})/dx$ from the data measured at the sparsely x -spaced stations.

Figure 17 displays the measured Reynolds shear stress data normalized by their maximum values, revealing that the shapes of Reynolds shear stress profiles approach a universal curve in the far field, irrespective of the pressure gradient. This phenomenon was first reported by Liu *et al.*¹² The figure confirms that the self-similar shape of the Reynolds shear stress can be approximated as

$$\frac{R_{uv}}{|R_{uv}|_{\max}} \approx 1.92\eta e^{(-0.637\eta^2 - 0.056\eta^4)} = 1.92\eta U^*. \tag{28}$$

V. CONCLUSIONS

The paper fills some long-standing gaps regarding the scaling of turbulent wake flow with adverse (APG) and forward (FPG) pressure gradient. Table II summarizes the main results of the present work. The results demonstrate the usefulness of using a combination of integral and self-similarity analyses to gain a better understanding of wake behavior in the presence of pressure gradients.

One aim of the present work is to address the gap in previous research by focusing on the properties of the mean transverse velocity. A new analytical equation is derived here for the mean transverse velocity at the wake edge from the global integral of the mean continuity equation. Moreover, applying a self-similarity assumption for U^* , a new analytical equation is derived for the mean transverse velocity. The analytical equation of V is found to consist of three components: one due to the mean pressure gradient, one similar to that of ZPG wake, and one to match the mean transverse velocity at the wake edge. This decomposition provides a useful framework for understanding the mean transverse flow in planar turbulent wakes under pressure gradient and how it is related to different velocity scales.

From the integral of the mean momentum equation, a new analytical equation for the Reynolds shear stress is derived, consisting of four components. By breaking down the Reynolds shear stress into its individual components, it may be possible to gain a deeper understanding of the flow dynamics and develop more accurate models of planar turbulent wakes. The findings of this work provide convenient theoretical tools for quick estimate of the planar turbulent wake development in pressure gradients, enable insights into possible ways of

further studies on the properties of planar turbulent wakes, and might be useful in various practical applications such as the design of wind turbines and the optimization of airfoils for aerospace applications.

AUTHOR DECLARATIONS

Conflict of Interest

The authors have no conflicts to disclose.

Author Contributions

Tie Wei: Conceptualization (equal); Data curation (equal); Formal analysis (equal); Investigation (equal); Methodology (equal); Project administration (equal); Validation (equal); Visualization (equal); Writing – original draft (equal); Writing – review & editing (equal). **Xiaofeng Liu:** Data curation (equal); Formal analysis (equal); Validation (equal); Writing – review & editing (equal). **Zhaorui Li:** Conceptualization (equal); Formal analysis (equal); Methodology (equal); Validation (equal); Writing – review & editing (equal). **Daniel Livescu:** Formal analysis (equal); Validation (equal); Writing – review & editing (equal).

DATA AVAILABILITY

Data sharing is not applicable to this article as no new data are reported in this study. The experimental data of Liu are available from https://turbmodels.larc.nasa.gov/Other_exp_Data/wake_planar_exp.html.

APPENDIX A: DETAILS OF INTEGRAL ANALYSIS

1. Volume and kinematic momentum flow rate in a planar turbulent wake

The volumetric flow rate $\dot{\gamma}$ and momentum flow rate \dot{M} in a planar turbulent wake are important quantities in the integral analysis of the mean continuity and momentum equations. The flow rates $\dot{\gamma}$ and \dot{M} per unit length in the spanwise direction in a planar turbulent wake are

$$\dot{\gamma} \stackrel{\text{def}}{=} \int_{-\delta_e}^{\delta_e} U dy = 2 \int_0^{\delta_e} U dy, \tag{A1a}$$

$$\dot{\mathcal{M}} \stackrel{\text{def}}{=} \int_{-\delta_e}^{\delta_e} U^2 dy = 2 \int_0^{\delta_e} U^2 dy. \quad (\text{A1b})$$

It is observed that the normalized mean axial velocity deficit $U^* = (U_e - U)/(U_e - U_{\text{ctr}})$ in the far field of a planar turbulent wake approaches a self-similar function of $y/\delta_{0.5}$ or y/δ_e (see Fig. 7). Employing the self-similarity property of U^* , two parameters I_1 and I_2 are defined using the integral of the first and second moments of the normalized mean streamwise velocity,

$$I_1 \stackrel{\text{def}}{=} \frac{1}{2\delta_e} \int_{-\delta_e}^{\delta_e} \frac{U_e - U}{U_e - U_{\text{ctr}}} dy = \frac{1}{\delta_e} \int_0^{\delta_e} \frac{U_e - U}{U_e - U_{\text{ctr}}} dy, \quad (\text{A2a})$$

$$I_2 \stackrel{\text{def}}{=} \frac{1}{2\delta_e} \int_{-\delta_e}^{\delta_e} \left(\frac{U_e - U}{U_e - U_{\text{ctr}}} \right)^2 dy = \frac{1}{\delta_e} \int_0^{\delta_e} \left(\frac{U_e - U}{U_e - U_{\text{ctr}}} \right)^2 dy. \quad (\text{A2b})$$

Note that the I_1 and I_2 defined here are essentially identical to the I_n defined by Townsend,² and no self-similarity assumption is made for the mean axial velocity deficit. Figure 18 presents the normalized mean axial velocity deficit and the integral of its first and second moments vs the normalized transverse location. The data points are from experimental measurements of Liu¹¹ (ZPG wake at $x = 48$ in.).

As shown in Sec. IV, the mean axial velocity deficit profiles reach a self-similarity state in the far field of planar turbulent wakes, and the self-similar Eq. (10) for U^* is represented by the solid curve in Fig. 18. The definitions of I_1 and I_2 can be re-written as $I_1 = \int_0^{\delta_e} U^* d(y/\delta_e)$ and $I_2 = \int_0^{\delta_e} (U^*)^2 d(y/\delta_e)$. Estimating the wake edge as the location of $U^* \approx 0.025$, it is determined that $\delta_e \approx 2.05\delta_{0.5}$. Note that the horizontal axis in Fig. 18 is $\eta = y/\delta_{0.5}$, so there is a factor of 2.05 in the integrated values shown by the dashed and dot-dashed curves. The values for I_1 and I_2 are $I_1 \approx 0.5$ and $I_2 \approx 0.36$, respectively.

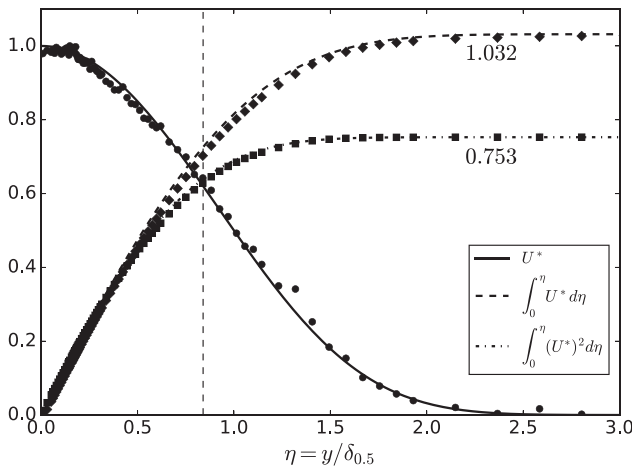


FIG. 18. Normalized mean axial velocity deficit $U^* = (U_e - U)/(U_e - U_{\text{ctr}})$ and integrals. The experimental data are from the ZPG case of Liu¹¹ at $x = 48$ in. The lines are based on the approximated $U^* = \exp(-0.637\eta^2 - 0.056\eta^4)$. The dashed vertical line marks the location of the maximum Reynolds shear stress $y_m \approx 0.84\delta_{0.5}$.

Using the definitions of I_1 and I_2 , the volumetric and kinematic momentum flow rate of the wake can be written as

$$\dot{\mathcal{V}} = 2 \int_0^{\delta_e} U dy = 2[U_e \delta_e - (U_e - U_{\text{ctr}})\delta_e I_1], \quad (\text{A3a})$$

$$\begin{aligned} \dot{\mathcal{M}} &= 2 \int_0^{\delta_e} U^2 dy \\ &= 2 \left[U_e^2 \delta_e - 2U_e(U_e - U_{\text{ctr}})\delta_e I_1 + (U_e - U_{\text{ctr}})^2 \delta_e I_2 \right]. \end{aligned} \quad (\text{A3b})$$

In the integration of the mean continuity and momentum equation to the maximum Reynolds shear stress location y_m , two parameters, I_{1m} and I_{2m} , are defined using the integral of the mean axial velocity deficit as

$$I_{1m} \stackrel{\text{def}}{=} \frac{1}{y_m} \int_0^{y_m} \frac{U_e - U}{U_e - U_{\text{ctr}}} dy, \quad (\text{A4a})$$

$$I_{2m} \stackrel{\text{def}}{=} \frac{1}{y_m} \int_0^{y_m} \left(\frac{U_e - U}{U_e - U_{\text{ctr}}} \right)^2 dy. \quad (\text{A4b})$$

Approximating U^* with Eq. (10), it is found that (see Fig. 18)

$$I_{1m} = 0.86; \quad I_{2m} = 0.76 \quad (\text{A5})$$

2. Global integrals of the mean continuity equation

Integrating the mean continuity Eq. (1a) from the wake centerline to the wake edge and applying boundary conditions yields

$$0 = \int_0^{\delta_e} \frac{\partial U}{\partial x} dy + (V_e - 0). \quad (\text{A6})$$

Note that the mean transverse velocity at the wake centerline is zero, due to the flow symmetry. Applying Leibniz's integral rule, the global integral of $\partial U/\partial x$ can be presented as

$$\int_0^{\delta_e} \frac{\partial U}{\partial x} dy = \frac{d}{dx} \int_0^{\delta_e} U dy - U_e \frac{d\delta_e}{dx} = \frac{d(0.5\dot{\mathcal{V}})}{dx} - U_e \frac{d\delta_e}{dx}. \quad (\text{A7})$$

Hence, the mean transverse velocity at the wake edge is

$$V_e = U_e \frac{d\delta_e}{dx} - \frac{d(0.5\dot{\mathcal{V}})}{dx} = \frac{d}{dx} \{ U_e \delta_e - 0.5\dot{\mathcal{V}} \} - \delta_e \frac{dU_e}{dx}. \quad (\text{A8})$$

Substituting $\dot{\mathcal{V}}$ from Eq. (A3a) into Eq. (A8), the mean transverse velocity at the wake edge can be written as

$$V_e = \frac{d}{dx} \{ (U_e - U_{\text{ctr}})\delta_e I_1 \} - \delta_e \frac{dU_e}{dx}. \quad (\text{A9})$$

In a ZPG wake, U_e is a constant and $(U_e - U_{\text{ctr}})\delta_e$ is also a constant [see Eq. (8)]. Thus, Eq. (A9) reproduces $V_e = 0$ for a ZPG wake.

3. Global integrals of the mean momentum equation

It can be shown that the global integral of $\nu \partial^2 U/\partial x^2$ is negligible for a planar turbulent wake. The global integral of $\nu \partial^2 U/\partial y^2$ from the wake centerline to the edge is $\nu \partial U/\partial y|_{\delta_e} - \nu \partial U/\partial y|_0$,

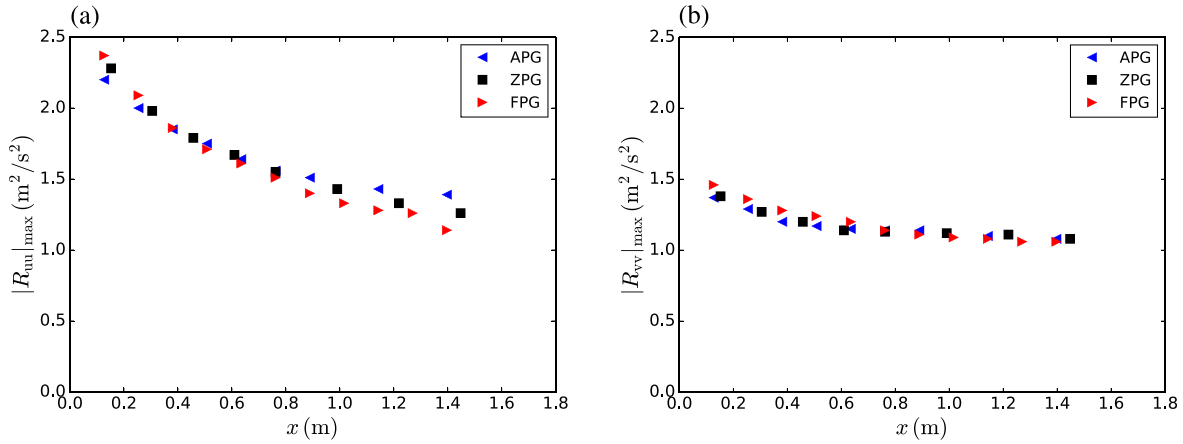


FIG. 19. Effects of pressure gradient on the maximum Reynolds normal stresses: (a) $|R_{uu}|_{\max}$ vs x , and (b) $|R_{vv}|_{\max}$ vs x , data are from experimental measurements of Liu.¹¹

equating zero from the boundary conditions. Thus, the global integration of the mean momentum Eq. (1b) from the wake centerline to the edge is

$$0 = - \int_0^{\delta_e} \frac{\partial U^2}{\partial x} dy - (U_e V_e - 0) - \int_0^{\delta_e} \frac{1}{\rho} \frac{dP_\infty}{dx} dy + \int_0^{\delta_e} \frac{\partial(R_{uu} - R_{vv})}{\partial x} dy + (R_{uv}|_{\delta_e} - 0). \quad (A10)$$

Note that V and R_{uv} are zero at the wake centerline due to the flow symmetry, and the Reynolds shear stress at the wake edge is also zero, $R_{uv}|_{\delta_e} = 0$.

Applying Leibniz’s integral rule, the first and the fourth integrals in Eq. (A10) can be presented as follows:

$$\int_0^{\delta_e} \frac{\partial U^2}{\partial x} dy = \frac{d}{dx} \int_0^{\delta_e} U^2 dy - U_e^2 \frac{d\delta_e}{dx} = \frac{d(0.5\dot{\mathcal{M}})}{dx} - U_e^2 \frac{d\delta_e}{dx}. \quad (A11)$$

and

$$\int_0^{\delta_e} \frac{\partial(R_{uu} - R_{vv})}{\partial x} dy = \frac{d}{dx} \int_0^{\delta_e} (R_{uu} - R_{vv}) dy - (R_{uu} - R_{vv})|_{\delta_e} \frac{d\delta_e}{dx}. \quad (A12)$$

Note that Reynolds normal stresses at the wake edge are zero: $(R_{uu} - R_{vv})|_{\delta_e} = 0$. Figure 2 shows that $U > 18$ (m/s) or $U^2 > 324$ (m^2/s^2), but Fig. 19 shows that R_{uu} and R_{vv} are both smaller than 2 (m^2/s^2) and $R_{uu} - R_{vv}$ is even smaller. Thus, it is reasonable to surmise that $\frac{d}{dx} \int_0^{\delta_e} (R_{uu} - R_{vv}) dy \ll \frac{d}{dx} \int_0^{\delta_e} U^2 dy$. Accordingly, the fourth term in Eq. (A10) can be neglected.

Substituting V_e from Eqs. (A8) and (A11) into Eq. (A10), the global integral of the mean momentum equation can be written as

$$0 = - \frac{d(0.5\dot{\mathcal{M}})}{dx} + U_e \frac{d(0.5\dot{\gamma})}{dx} - \int_0^{\delta_e} \frac{1}{\rho} \frac{dP_\infty}{dx} dy. \quad (A13)$$

If the mean pressure gradient $d(P/\rho)/dx$ does not vary in the transverse direction, the global integral of the mean momentum equation can be simplified as

$$0 = - \frac{d(0.5\dot{\mathcal{M}})}{dx} + U_e \frac{d(0.5\dot{\gamma})}{dx} + U_e \delta_e \frac{dU_e}{dx} = \frac{d}{dx} \{0.5(U_e \dot{\gamma} - \dot{\mathcal{M}})\} + \{U_e \delta_e - 0.5\dot{\gamma}\} \frac{dU_e}{dx}. \quad (A14)$$

Substituting $\dot{\gamma}$ from Eq. (A3a) and $\dot{\mathcal{M}}$ from Eq. (A3b) into Eq. (A14), the global integral of the mean momentum equation can be written as

$$0 = \frac{d}{dx} \{U_e(U_e - U_{ctr})\delta_e I_1 - (U_e - U_{ctr})^2 \delta_e I_2\} + (U_e - U_{ctr})\delta_e I_1 \frac{dU_e}{dx}. \quad (A15)$$

Note that all the variables in Eq. (A15) are determined from the measurements of the mean axial velocity profiles at multiple axial locations.

APPENDIX B: NORMALIZE THE MEAN TRANSVERSE VELOCITY BY $|(U_e - U_{ctr})d\delta_{0.5}/dx|$

In Fig. 12, the normalized mean transverse velocity in the free stream has a slope of 1 (for APG wake) or -1 (for FPG wake) because the mean transverse velocity in Eq. (17) is normalized by $|a_1|$. As a_1 approaches zero (ZPG wake), it is better to normalize the mean transverse velocity by $|a_{III}|$, instead of $|a_1|$. The dimensionless mean transverse velocity normalized by $|a_{III}| = |(U_e - U_{ctr})d\delta_{0.5}/dx|$ can be expressed as

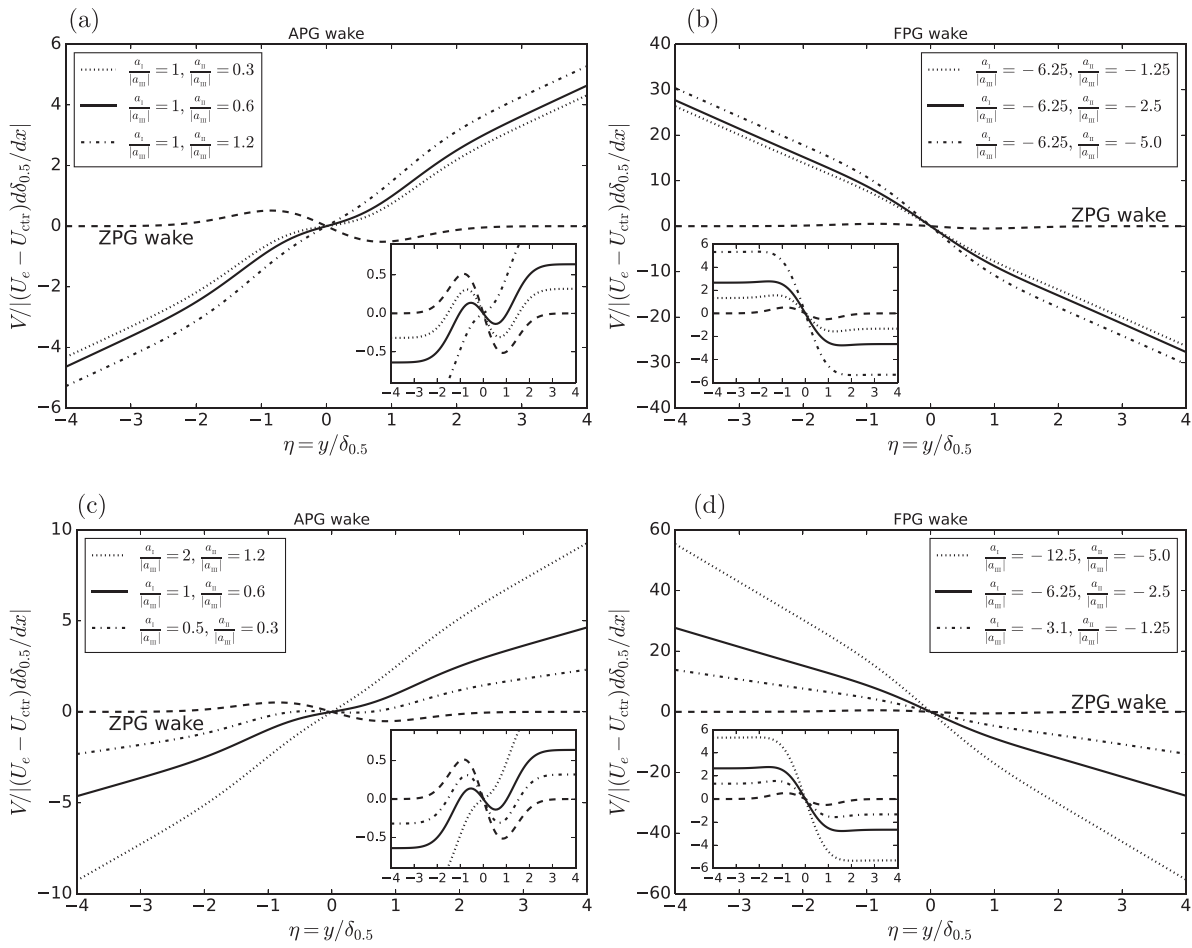


FIG. 20. Mean transverse velocity profile normalized by $|a_{III}| = |(U_e - U_{ctr})d\delta_{0.5}/dx|$: (a) APG wake with different $a_{II}/|a_{III}|$; (b) FPG wake with different $a_I/|a_{III}|$ and $a_{II}/|a_{III}|$; (c) APG wake with different $a_I/|a_{III}|$ and $a_{II}/|a_{III}|$; and (d) FPG wake with different $a_I/|a_{III}|$ and $a_{II}/|a_{III}|$. The insets show the sum of the last two terms in Eq. (B1) (without the linear function). The dashed curve represents the mean transverse flow in a ZPG wake, and the other three curves correspond to the curves in Fig. 12.

$$\frac{V}{|(U_e - U_{ctr}) \frac{d\delta_{0.5}}{dx}|} = \frac{-\delta_{0.5} \frac{dU_e}{dx}}{|(U_e - U_{ctr}) \frac{d\delta_{0.5}}{dx}|} \eta + \frac{\frac{a_I/|a_{III}|}{dx} d[(U_e - U_{ctr})\delta_{0.5}]}{|(U_e - U_{ctr}) \frac{d\delta_{0.5}}{dx}|} \frac{\sqrt{\pi}}{2\sqrt{a}} \operatorname{erf}(\sqrt{a}\eta) + \frac{\frac{a_{II}/|a_{III}|}{dx} d\delta_{0.5}}{|(U_e - U_{ctr}) \frac{d\delta_{0.5}}{dx}|} \eta \exp(-a\eta^2). \tag{B1}$$

Figure 20 presents the mean transverse velocity profile normalized by $|a_{III}|$. The three curves in Fig. 20 use the same a_I , a_{II} , and a_{III} as the corresponding ones in Fig. 12. That is, the mean transverse flow V in Fig. 20 is identical to the corresponding one in Fig. 12, except that V is normalized by a_{III} , and a_I , respectively.

Figures 20(a) and 20(b) present the effect of $a_{II}/|a_{III}|$ on the shape of $V/|a_{III}|$. As $a_I/|a_{III}|$ is kept at a constant, the slope of the mean transverse flow in the free stream remains fixed. As the magnitude of $a_{II}/|a_{III}|$ increases, the mean transverse flow within the wake deviates more from that in a ZPG wake, and the $V/|a_{III}|$ tilts further from the linear function $y\partial V/\partial y|_e$.

In Fig. 20(c) and 20(d), the ratio $a_{II}/|a_{III}|$ is kept at a constant [see Figs. 20(c) and 20(d)], but both $a_I/|a_{III}|$ and $a_{II}/|a_{III}|$ vary. As the magnitude of $a_I/|a_{III}|$ increases, the slope of $V/|a_{III}|$ in the free stream becomes steeper, and the mean transverse flow inside the wake also deviates more from that in a ZPG wake.

APPENDIX C: CURVE-FITTING AND ERROR PROPAGATION

Inevitably, the measured data of δ_{05} , U_e , and $U_e - U_{ctr}$ contain errors. These errors will propagate to derived quantities through the addition and the multiplication of the measured quantities and the calculation of the x -derivatives, such as $d\delta_{05}/dx$, dU_e/dx , or $d(U_e - U_{ctr})/dx$. To account for the influence of the error propagation, the measured profiles of δ_{05} , U_e , and $U_e - U_{ctr}$ in the axial direction were first curve-fitted using a power law ax^b or an exponential law $a \exp(bx)$ based on the established consensus on the streamwise variations of these quantities. The curve-fitted functions are then used in the calculation of V_e Eq. (3), global momentum balance Eq. (4), maximum R_{uv} Eq. (9), and a_I , a_{II} , and a_{III} in Eq. (14). The calculation of the error bar is similar to the multi-variable error propagation described by Figliola and Beasley.²⁴ In the present work, δ_{05} , U_e , and $U_e - U_{ctr}$ are taken as the independent variables for a derived variable R (for example, V_e), and the uncertainty of R at the k th measuring station is calculated as

$$u_R|_k = \sqrt{\left(\frac{\partial R}{\partial \delta_{05}} \Big|_k u_{\delta_{05}}\right)^2 + \left(\frac{\partial R}{\partial U_e} \Big|_k u_{U_e}\right)^2 + \left(\frac{\partial R}{\partial (U_e - U_{ctr})} \Big|_k u_{(U_e - U_{ctr})}\right)^2}, \quad (C1)$$

where $u_{\delta_{05}}$, u_{U_e} , and $u_{(U_e - U_{ctr})}$ are the rms calculated from the curve-fitted and measured δ_{05} , U_e , and $U_e - U_{ctr}$ over the x -stations in the fully developed region.

REFERENCES

- ¹H. Schlichting, *Boundary-Layer Theory*, 7th ed. (McGraw-Hill Book Company, New York, 1979).
- ²A. Townsend, *The Structure of Turbulent Shear Flow* (Cambridge University Press, 1980).
- ³S. Pope, *Turbulent Flows* (Cambridge University Press, 2000).
- ⁴E. Guseva, M. Shur, M. Strelets, A. Travin, W. Breitenstein, R. Radespiel, P. Scholz, M. Burnazzi, and T. Knopp, "Experimental/numerical study of turbulent wake in adverse pressure gradient," in *Progress in Hybrid RANS-LES Modelling: Papers Contributed to the 7th Symposium on Hybrid RANS-LES Methods, 17–19 September, 2018, Berlin, Germany* (Springer, 2020), pp. 401–412.
- ⁵F. Porté-Agel, M. Bastankhah, and S. Shamsoddin, "Wind-turbine and wind-farm flows: A review," *Boundary-layer Meteorol.* **174**, 1–59 (2020).
- ⁶C. Lav, J. Philip, and R. D. Sandberg, "Compressible plane turbulent wakes under pressure gradients evolving in a constant area section," *J. Fluid Mech.* **892**, A35 (2020).
- ⁷J. P. Slotnick and D. Mavriplis, "A grand challenge for the advancement of numerical prediction of high lift aerodynamics," AIAA Paper No. 2021-0955, 2021.
- ⁸I. S. Gartshore, "Two-dimensional turbulent wakes," *J. Fluid Mech.* **30**, 547–560 (1967).
- ⁹R. Narasimha and A. Prabhu, "Equilibrium and relaxation in turbulent wakes," *J. Fluid Mech.* **54**, 1–17 (1972).
- ¹⁰M. Tummers, D. Passchier, and R. Henkes, "Experimental investigation of an adverse pressure gradient wake and comparison with calculations," *Exp. Therm. Fluid Sci.* **14**, 17–24 (1997).
- ¹¹X. Liu, "A study of wake development and structure in constant pressure gradients," Ph.D. thesis (University of Notre Dame, 2001).
- ¹²X. Liu, F. Thomas, and R. Nelson, "An experimental investigation of the planar turbulent wake in constant pressure gradient," *Phys. Fluids* **14**, 2817–2838 (2002).
- ¹³X. Liu and F. Thomas, "Measurement of the turbulent kinetic energy budget of a planar wake flow in pressure gradients," *Exp. Fluids* **37**, 469–482 (2004).
- ¹⁴F. Thomas and X. Liu, "An experimental investigation of symmetric and asymmetric turbulent wake development in pressure gradient," *Phys. Fluids* **16**, 1725–1745 (2004).
- ¹⁵D. M. Driver and G. G. Mateer, "Wake flow in adverse pressure gradient," *Int. J. Heat Fluid Flow* **23**, 564–571 (2002).
- ¹⁶D. M. Driver and G. G. Mateer, "Evolution of a planar wake in adverse pressure gradient," Technical Report No. NASA/TM-2016-219068, 2016.
- ¹⁷P. Spalart and S. Allmaras, "A one-equation turbulence model for aerodynamic flows," AIAA Paper No. 92-0439, 1992.
- ¹⁸F. Menter, "Zonal two equation $k - \omega$ turbulence models for aerodynamic flows," in *23rd Fluid Dynamics, Plasmadynamics, and Lasers Conference* (AIAA, 1993), p. 2906.
- ¹⁹T. von Kármán, "Über laminare und turbulente reibung," *J. Appl. Math. Mech./Z. Angew. Math. Mech.* **1**, 233–252 (1921).
- ²⁰K. Pohlhausen, "Zur näherungsweise integration der differentialgleichung der laminaren grenzschicht," *J. Appl. Math. Mech./Z. Angew. Math. Mech.* **1**, 252–290 (1921).
- ²¹T. Wei, D. Livescu, and X. Liu, "Scaling patch analysis of planar turbulent wake," *Phys. Fluids* **34**, 065116 (2022).
- ²²I. Wygnanski and H. Fiedler, *Some Measurements in the Self Preserving Jet* (Cambridge University Press, 1968).
- ²³W. George, "The self-preservation of turbulent flows and its relation to initial conditions and coherent structures," in *Advances in Turbulence* (Springer, 1989), pp. 39–73.
- ²⁴R. S. Figliola and D. E. Beasley, *Theory and Design for Mechanical Measurements* (John Wiley & Sons, 2020).